Formation and sealing processes of underground-water conducting fractures associated with faulting of granite

（地下花崗岩体中の断層に伴う透水性割れ目の

形成・シーリングプロセス）

石　橋　　正　祐　紀

2016

Formation and sealing processes of underground-water conducting fractures associated with faulting of granite

（地下花崗岩体中の断層に伴う透水性割れ目の

形成・シーリングプロセス）

ISHIBASHI, Masayuki

(石橋　正祐紀)

A dissertation for the degree of Doctor of Science

Department of Earth and Environmental Sciences,

Graduate School of Environmental Study, Nagoya University

（名古屋大学大学院環境学研究科地球環境科学専攻学位論文　博士（理学））

2016 年

Contents:

Abstract

Fractures and fractured zones developed along faults (i.e., damage zones) provide pathways for groundwater flow and solute transportation in granitic rocks. Granitic rock fractures are distributed in orogenic belts such as the Japanese islands rather than in stable continental crust, suggesting that the cooling and uplifting processes of granitic rocks differ in orogenic belts and continental crust. However, the features of groundwater-conducting fractures (WCFs) formed along granitic rock faults in orogenic belts have not been well characterized. Understanding the formation process and longevity of these fractures as well as their *in situ* hydrological features is crucial for the safety assessment of underground usages such as underground liquefied petroleum gas (LPG) storage and high-level radioactive waste (HLW) repositories. To reveal the detailed *in situ* characteristics and the long-term behavior of WCFs along the faults in granitic rocks, this study investigated the geological, mineralogical, and hydrological features of the Toki granitic rock excavated up to a depth of 500 m in central Japan. The investigations were performed at the Mizunami Underground Research Laboratory (MIU).

From *in situ* detailed observations, mineralogical analysis and hydraulic measurements across the fault distributed in the underground rock, I revealed the distinctive spatial characteristics of the fractures, i.e., their distributions, fillings, and orientations, the fractures closely associated with groundwater inflows, and the hydraulic transmissivity in and around a fault-damaged zone. The relatively long fractures (longer than approximately 4 m) that are readily traceable across the gallery appear with nearly equal frequency within the damage zone and host rock, whereas shorter fractures (under approximately 4 m) are far more common in the damage zone.

The filling minerals also differ between the longer and shorter fractures. The longer fractures are filled with multiple layered minerals, such as chlorite and sericite, formed by groundwater circulation at relatively high temperature, probably during the cooling of pluton and uplifting. The shorter fractures are usually filled with single minerals, such as calcite, which are formed due to reaction with penetrated surface water. Clayey-type fillings (mainly fine-grained calcite and smectite) are uniquely observed in the damaged zone, suggesting their injection by high-pressure pore water due to fault movements. Present *in situ* hydraulic measurements confirmed the lower permeability of the damaged zone than that of fractured host rock. From these geological observation and *in situ* measurements, I inferred three stages of fracture formation in and along the granitic rock fault.

First stage (Stage I): Background fractures (the relatively long fractures identified in the host rock) formed after the temperature decreased to the ductile–brittle transition. Most of these fractures were formed under brittle deformation conditions that preceded the fault development. Layered fracture fillings were also mainly developed in this stage due to thermal water circulation.

Second stage (Stage II): The damage zone formed along the fault. Shorter fractures with network formations and easily distinguishable morphological features were developed in this zone.

Third stage (Stage III): The fractures were filled and sealed by clayey type fillings, probably under continuous faulting activities, which reduced the hydraulic permeability of the damaged zone. Today, nearly 90% of the fractures are sealed by fillings and the damage zone has lost its water-conductive function.

The study results show that even if many fractures formed after cooling and faulting

of granitic rock in the damage zone, most of these fractures no longer admit groundwater flow, as they are filled with minerals formed by groundwater circulation as well as fault reactivation in the granitic rocks distributed in an active orogenic field of Japan.

Chapter 1: Background

1-1. Introduction

Fractures and fractured zones around faults (i.e., mechanical “damage zones”) in granitic rocks provide pathways for groundwater flow and solute transportation (Nagra, 1994; Mazurek et al., 2003; Yoshida et al., 2002, 2005, 2013a, 2013b; SKB, 2006a; Ishibashi et al., 2014). Damage zones with interconnected fracture networks developed along the faults are especially important hydrogeological structures, because they form the main conduits from deep underground regions to the ground surface (Fig. 1; Chester et al., 1993; JNC, 2000a; Mazurek et al., 2003; SKB, 2006; Faulkner et al., 2010; Yoshida et al., 2014). In active orogenic fields such as the Japanese islands, smaller scale faults (approximately a few hundred meters to several km) are inevitably distributed throughout deep host rocks and occur at intervals of several hundred meters (Yoshida et al., 2013a; Ishibashi et al., 2013; Sakai et al., 2016). Such smaller scale faults and their associated fracture network enhance the hydrological and elemental migration through deep host rocks. Understanding the fractures and damage zones in underground environments is important for safety assessments of underground facilities, such as those used in high-level radioactive waste (HLW) disposal and liquefied petroleum gas (LPG) storage (Yoshida, 2012; Yoshida et al., 2013; Ishibashi et al., 2014). Especially in underground HLW disposal, the usage capability is required for several hundred thousand years (IAEA, 1983a; JNC, 2000a; Yoshida, 2012). To understand the behavior of fractures and damage zones, many researchers have described their surface outcrops and conducted underground investigations (Keusen et

al., 1989; Nagra, 1994; JNC, 2000a; Mazurek et al., 2003; SKB, 2006a; Sawada et al., 2015). Several numerical and conceptual models have been constructed from detailed investigations of the boreholes and galleries in underground facilities. Faults are water-conductive, as confirmed at the Grimsel Test Site in the central-area massif of the Swiss Alps, the Äspö Hard Rock Laboratory in southeast Sweden, and ONKALO in western Finland (Fig. 2; Keusen et al., 1989; Nagra, 1994; Mazurek et al., 2003; SKB, 2006a; Follin et al., 2007; Sawada et al., 2015). However, the geological characterizations of the fractures and damage zones differ between surface investigations and underground studies. Moreover, the characteristics of the water-conducting fractures (WCFs) differ between orogenic fields and stable continental regions (Yoshida et al., 2005, 2013b). For example, in orogenic fields such as the Japanese islands, WCFs comprise approximately 10% of all observed fractures, because most of the fractures are filled with sealant minerals formed by water/rock interactions, although orogenic fields contain more fractures overall than stable continental regions such as Europe and the United States (Yoshida, 2012; Ishibashi et al., 2014). In addition, the cooling and uplift rates of granitic rocks differ between orogenic and continental fields (SKB, 2008; Yamasaki et al., 2012; Sasao et al., 2005). To understand how the long-term behavior of fractures and damage zones relates to their role as WCFs, and hence derive the actual features of WCFs developed in the granitic rock distributed through Japanese orogenic field, I require *in situ* investigations of the underground environments. For the first time, this study demonstrates the long-term behavior and characteristics of fractures in an orogenic underground environment. The investigation is based on data obtained at the Mizunami Underground Research Laboratory (MIU) site in central Japan.

1-2. Water-conducting fractures in underground environments

Modeling of fracture networks in groundwater flow analysis has progressed since the 1970s (Witherspoon and Gale, 1977; Witherspoon, 1979; Narashimhan, 1982), and analytical methods for hydraulic and mass transportation and models for underground environments have advanced since the 1980s (Grink, 1993; Nagra, 1985). In the 1990s, researchers began detailed investigations of WCFs (Allen and Simmons, 1996; SKB, 1995), revealing the structures of the flow channels in fractures and the retardation functions in underground scenarios (Neretnieks, 1990; Grink, 1993). After the 1990s, a series of *in situ* experiments was started in the Kamaishi mine in Iwate Prefecture, northern Japan (JNC, 1999, 2000a; Mikake et al., 2000). These studies revealed that WCFs comprise only 40% of the Kamaishi mine fractures, and form a channel structure with heterogeneously located inflow points in a single fracture (JNC, 1999, 2000a; Yoshida et al, 2000, 2002). Moreover, carbonate filling in the fractures proved a useful indicator of WCF (Alexander et al., 2000; Blyth et al., 2000; Iwatsuki et al., 2002; Degnan and Bath, 2005) and the fault damage zones act as significant WCFs (Fig. 1; Rhén et al., 2003; Faulkner et al, 2010). However, these studies focused only on the current conditions of the WCFs. The long-term behavior of WFCs in underground environments has gained attention only recently (Yoshida et al., 2009, 2013b; SKB 2006a, 2011, 2014). The frequency of “background fractures” (Vermilye and Scholz, 1998; Yoshida et al., 2009), which are not related to faults, is now thought to be nearly constant in the granitic rocks of the Japanese islands, irrespective of their ages and locations. This indicates that background fractures are formed shortly after solidification to retain the strain within the pluton. Thereafter, few fractures are formed even when the

pluton is subjected to regional stresses by plate movements (Yoshida et al., 2005, 2013b). In addition, investigations of sub-solidus structures have shown that the fracture distribution is affected by the local cooling rate of granitic rock at the sub-solidus temperature (approximately 500 °C; Yuguchi et al., 2012).

Table 1 summarizes the features of representative granitic rocks in a stable Continental region (Forsmark in Sweden (Follin, 2008) and Olkiloto in western Finland (Aaltonen et al., 2016)) and in an active orogenic field (the MIU site in this study). Forsmark was the first geological HLW disposal site worldwide (Fig. 2). The granitic rocks at Forsmark and Olkiluoto are approximately 2 Ga old (Follin, 2008; Aaltonen et al., 2016), more than thirty times older than the late Cretaceous granitic rocks at the MIU site (approximately 70 Ma; Suzuki and Adachi, 1998). The late Cretaceous granitic rocks are widely distributed in the Japanese islands (Yasue et al., 2014), and their fracture frequency is twice to fourfold that of granitic rock in Forsmark and Olkiluoto (Table 1; Follin et al., 2007; Hartley et al., 2013; Saegusa et al., 2015). In Forsmark and Olkiluoto, the fracture frequency and permeability is high in the upper part of the granite and decreases with depth from the ground surface (Fig. 2; Follin et al., 2007; Hartley et al., 2013). Meanwhile, the fault frequency at the MIU site is approximately tenfold and threefold of that at the Forsmark and Olkiluoto sites, respectively (Follin, 2008; Hartley et al., 2013; Ishibashi et al., 2013; Sakai et al, 2016). The cooling rate when the background fractures formed around the ductile–brittle transition temperature (300 °C–370 °C; Matsushima and Okubo, 2003; Sasada and Sasaki, 2004) is slower at the Continental sites than at the MIU site (SKB, 2008; Aaltonen et al., 2016; Yamasaki et al., 2012). This indicates that granitic rocks cool more slowly in Sweden and Finland than in Japan, although whether this difference directly relates to the difference in

fracture frequency is unclear. The present-day uplift rate is faster at Forsmark and Olkiluoto than at the MIU site (SKB, 2008; Sasao et al., 2005), because deglaciation at the North European sites reduces the vertical stress (SKB, 2008). Consequently, the highly permeable WCFs in Forsmark arose from low-angle fractures in the upper part of the granitic rock (Fig. 2; SKB 2006a, 2014; SKB, 2010). Deglaciation is thus an important driver of the long-term evolution of Sweden's underground environment (SKB, 2008). This feature is unique to Sweden and differs from the features of the Japanese islands, where few glaciations have occurred.

The distribution of faults and fractures in the underground environments of the Japanese islands distinctly differ from those in stable continental regions, because the cooling and uplifting of the granitic bodies occur by different processes in the two environments. The Japanese islands feature smaller-scale faults (approximately a few hundred meters to km) spaced by a few hundred meters (Yoshida et al., 2013a; Ishibashi et al., 2013; Sakai et al., 2016). Such smaller scale faults and their associated fracture network (i.e., damage zone) encourage hydrological and elemental migration in the deep host rocks. However, the influence of faulting on the long-term behavior of the WCF and damage zone is poorly understood in active orogenic fields such as the Japanese islands. This thesis describes the long-term behavior of damage zones and their realistic features forming the hydrogeological structure in the underground environment.

1-3. Geological setting around the MIU site and study area

The MIU project, conducted by the Japan Atomic Energy Agency in Mizunami City,

Gifu Prefecture, central Japan (Fig. 3a), primarily aims to establish methodologies for investigating, analyzing, and assessing deep geological environments. Ultimately, the project will guide research and development on the geological disposal of HLW. The underground MIU facilities include two vertical shafts (a main shaft and a ventilation shaft), connected by horizontal tunnels at 100-m depth intervals. Measurement niches are placed at 200 m and 300 m below ground level, and access/research galleries reside at 300 m and 500 m below ground level (see Fig. 3b). Both shafts are approximately 500 m below the ground surface. Their elevation ranges from 200.9 m at the surface to −299.1 m at the shaft bottom. The shafts and galleries were constructed by the blast method.

The MIU site is situated on Miocene sedimentary rocks of the Mizunami Group, which unconformably overlie the Toki granite (Fig. 3a). The vertical shafts penetrate the Mizunami Group and enter the Toki granite through the unconformity at approximately 170 m below ground level. The Toki granite is part of the Late Cretaceous plutonic intrusive in the Sanyo Belt (Ishihara and Chappell, 2007).

The primary mineral assemblage in the Toki granite is quartz, plagioclase, and K-feldspar with accessory biotite and minor amounts of zircon, monazite, apatite, allanite, and opaque minerals (Nishimoto et al., 2008). The Toki granite has been aged as 68.3 ± 1.8 Ma using the monazite chemical Th–U–total Pb isochron method (CHIME) (Suzuki and Adachi, 1998), 72.3 ± 3.9 Ma by whole-rock Rb–Sr dating (Shibata and Ishihara, 1979), and 76.3 ± 1.5 Ma by mineral Rb–Sr dating (Nishimoto et al., 2014). Biotite K–Ar ages range from 78.5 ± 3.9 to 59.7 ± 1.5 Ma, and zircon fission-track (FT) dating yields similar ages, ranging from 75.6 ± 3.3 to 52.8 ± 2.6 Ma (Yuguchi et al., 2011). Apatite FT dating gives approximate ages of 32 to 49 Ma (Sasao

et al., 2015). These chronological data indicate a rapid cooling stage followed by a slow cooling stage of the Toki granite. During the rapid cooling stage (approximately 30 °C–70 °C/million years), monazite Pb to zircon FT closure occurred in the approximately 70–60 Ma range; during the slow cooling stage (approximately 3 °C–13 °C/million years), zircon FT to apatite FT closure occurred in the 60–40 Ma range (Sasao et al., 2015). Yamasaki and Umeda (2012) estimated the cooling rate of the rock body by thermochronology, and suggested that the Toki granite was exposed to the land surface between 33 and 24 Ma. The background fractures were formed during the rapid cooling stage of the Toki granite, and became extended (developed) by the stress released during uplift and denudation of the granitic rocks (Ishibashi et al., 2014). The fractures acted as WCFs and became infiltrated with hydrothermal fluid and/or relatively low-temperature water; consequently, they became filled or sealed with hydrothermal minerals (sericite and chlorite) and calcite (Nishimoto et al., 2008; Ishibashi et al., 2014).

The Miocene Mizunami Group (with a zircon fission-track age of 20–18 Ma; Sasao et al., 2006) is divided into three units by unconformities or disconformities. The oldest unit, the Toki lignite-bearing formation, is composed of fresh water sediments. The intermediate-age unit consists of two formations, the Hongo and the Akeyo, intercalated with fresh water and marine sediments. The youngest unit, the Oidawara Formation, comprises marine sediments (Itoigawa, 1974, 1980).

A nearly vertical fault striking N28°W–57°W (Main Shaft Fault) was mapped from approximately 10 m to 500 m below ground level in the main shaft. This is a major fault at the MIU site (Kuboshima et al., 2012; Tsuruta et al., 2013; Fig. 4). A smaller high-angle fault with a NNW–SSE strike (Small Fault) was mapped approximately 50 m from the Main Shaft Fault at 500 m below ground level (Kawamoto et al., 2014; Fig.

4b). The sense of the slip along the Main Shaft Fault is normal at the unconformity and strike-slip in the Toki granite (Kuboshima et al., 2012). The Main Shaft Fault has been reactivated and subjected to several distinct fault movements (Tagami et al., 2012). The fault core of the Main Shaft Fault in the Toki granite comprises several fault gouges, fault breccia, lamprophyre, and strongly altered granite (Fig. 5a). The Small Fault comprises only fault gouges (Kawamoto et al., 2014; Fig. 5b). The fault gouge of the Main Shaft Fault is approximately 0.73 m and 0.43 m thick at the 300 m and 500 m depths, respectively, whereas the Small Fault is 0.03 m thick (Kawamoto et al., 2012, 2013, 2014; Fig. 5). An alteration halo, characterized by biotite chloritization and plagioclase seritization, is observed on the wall rocks around the fractures (at several hundredths to several tenths of meters from the fractures themselves) near the Main Shaft Fault (Nishimoto and Yoshida, 2010; Ishibashi et al., 2014).

Horizontal galleries, extending northward or northeastward from the main shaft, were constructed at 300 m and 500 m below ground level with total gallery lengths of approximately 100 m and 165 m, respectively (Figs. 3b and 4). The Toki granite on the northeast side of the Main Shaft Fault was drilled with four horizontal boreholes (Borehole-A: 62.5 m, Borehole-B: 103 m, Borehole-C: 85.4 m, and Borehole-D: 110 m; total length 360.6 m) at 300 m below ground level (Fig. 4a), and with three horizontal boreholes (Borehole-E: 37 m, Borehole-F: 107 m, Borehole-G: 102.1 m; total length 346.1 m) at 500 m below ground level (Fig. 4b). The borehole directions, with bearings clockwise from North, are 19.6° (Borehole A), 358.2° (Borehole B), 260.7° (Borehole C), 279.5° (Borehole D), 39.5° (Borehole E), 349.8° (Borehole F), and 350.2° (Borehole G). At the 300 m depth, a relatively high groundwater inflow occurred during the drilling of Borehole-A, which was arrested by pre-excavation grouting to over 40 m

from the main shaft. Borehole-A was the pilot boring for construction of the gallery at that depth (Mikake et al., 2010).

Chapter 2: Methodology and data for fracture analysis

Borehole and geological investigations were conducted in the research galleries on the northeast side of the Main Shaft Fault at 300 m and 500 m below ground level (Table 2). This site was selected because all fractures on the research gallery wall have been mapped and hydrological information is available from the Main Shaft Fault to the zone of relatively low fracture density (host rock; Fig. 4). The dates of fracture distributions, fracture fillings, fracture orientations, fractures closely related to groundwater inflow, and hydraulic transmissivity were systematically obtained continuously from the Main Shaft Fault (Figs. 4, 6, and 7). As the main Shaft Fault is vertical, the effect of faulting was studied through the high- and middle-angle fractures (collectively called *fractures*).

2-1. Borehole investigations

The distributions of fracture frequencies, fracture orientations, and hydraulic transmissivity were determined by core logging, borehole television surveys, and hydraulic packer tests (Table 2).

The fracture frequency was calculated from the fracture data obtained in drill core and borehole television images, because natural fractures are not easily distinguished from artificial fractures induced by drilling.

The fracture orientations were obtained by borehole television survey, and their inherent bias (Terzaghi, 1965) was corrected by a Terzaghi weighting factor.

2-2. Geological investigations in the research galleries

After each blast round (approximately 1.6–1.7 m in length), the distributions of fracture frequencies, fracture orientations, filling mineralogy, and WCFs (fractures with groundwater inflow) were determined by geological investigations in the research galleries. The investigations were undertaken by two complementary methods. In the scan-line investigation, a tape measure was aligned parallel to the gallery axis (the scan-line) and the fractures and their characteristics (orientation and filling mineralogy) were recorded in the region crossed by the tape measure. The scan-line investigation was performed along both sides of the galleries at 300 m and 500 m below ground level. The scan-line was set at 1.25 or 2.50 m above the gallery floor, depending on the gallery size (Fig. 4). The other method was wall-rock mapping in the research galleries (gallery-wall mapping), sketching the observable fractures and obtaining the fracture trace length along the gallery wall, the WCF distribution, and the inflow rate (Table 2).

The trace length distribution indicates the fracture size distributions (Piggott, 1997), which correlate with the hydraulic permeability (Ijiri et al., 2001). The cumulative fracture trace lengths generally follow a power-law distribution (Turcotte, 1986; Scholz and Cowie, 1990; Ijiri et al., 2001). The processes of cutting off the longer and shorter portions of the fracture trace length are called *truncating* and *censoring*, respectively (Ijiri et al., 2001; Raymond and Svensk, 2004). Truncating biases the size of the observation domain, omitting some of the information. Especially, the number of each size of the large fractures depends on the size of the observation domain, as the large fracture planes may extend beyond the rock exposure. Censoring also omits information, as fractures shorter than some threshold value are physically impossible to detect. Given

that the cumulative distribution of the fracture trace lengths follows a power law in the range of 1.0–7.0 m, the *all fracture frequency* (Figs. 6c and 7s) was sampled by mapping the trace lengths within this range.

The WCFs were recorded as *wet* (less than 0.1 L/min), *dripping* (between 0.1 and 1.0 L/min), *flowing* (greater than 1.0 L/min), or *grouted*, denoting that the fractures are filled with grout. Grouted fractures were assumed as WCFs because their apertures were presumably sufficient to receive the grout materials.

Fracture fillings are useful indicators of past fluid flow and may illustrate the groundwater flow patterns (Yoshida et al., 2013b). Because the unconsolidated clayey fillings at the MIU site (Yoshida, 2012; Yoshida et al., 2013b) might have been washed out during the borehole drilling, the fracture filling mineralogy was investigated by the scan-line method.

The relation between the trace length and frequency distribution of the fractures was elucidated by multivariate analysis of the fracture frequencies measured in the gallery-wall mapping, which were normalized by Eq. (1). When estimating the expected values and their variances, I assumed an exponential distribution because the probability of the fracture frequency density follows this distribution (Fig. 8b).

$$f_n(x_i) = (x_i - E)/\sqrt{V} \qquad (1)$$

where $f_n(x_i)$ is the normalized fracture frequency, x_i is the fracture frequency per meter from the Main Shaft Fault, and E and V are the expected value and variance, respectively, of the exponential distribution. The normalized values calculated by Eq. (1) were input to the multivariate analysis.

2-3. Laboratory tests

Thin sections were observed by polarizing optical microscopy and X-ray diffraction (XRD) analyses. The occurrence, mineral species, and origin of the fracture fillings were determined from the oxygen and carbon isotopic ratios in the calcite.

The fracture fillings were drilled with a mini-drill to identify their contained minerals. The X-ray diffraction pattern was measured by an X-ray diffractometer (Ultima IV, Rigaku) operated at 20-kV CuKa radiation and 20 mA. The 2θ range was 2°–70° at 5°/min intervals.

The calcite samples were classified by their crystalline forms. After powdering with a mini-drill, they were converted to CO_2 gas by reacting with 100% phosphoric acid in a vacuum line. The O and C isotope ratios in the gas were determined by isotope ratio mass spectrometry (IsoPrime100 IRMS, Isoprime). The results are reported in the conventional δ-notation, adopting the Pee-Dee Belemnite (PDB) standard for $^{13}C/^{12}C$ and the Standard Mean Ocean Water (SMOW) standard for $^{18}O/^{16}O$. The isotopic oxygen compositions $\delta^{18}O$ are related to the PDB values as follows:

$$\delta^{18}O_{SMOW} = 1.03086\delta^{18}O_{PDB} + 30.86\ (‰)$$

(IAEA, 1983b).

Chapter 3: Fracture distributions around faults

3-1. Distributions of the fracture characteristics

In both the 300 m and 500 m deep galleries, the fractures strike predominantly in the NW–NNW, NE, and EW directions (Figs. 6a, 6b and 7a, 7b). The NW–NNW striking fractures dominate within approximately 80–100 m and 60 m from the Main Shaft Fault at depths of 300 m and 500 m, respectively. Beyond these distances, the 300 m and 500 m depths are largely populated by NE and EW striking fractures, respectively.

At the 300 m depth, the fracture frequencies measured by the wall mapping gradually decreased with distance from the Main Shaft Fault (Fig. 6c). However, the fracture frequencies measured by the scan-line and borehole investigations were relatively constant within 100 m of the fault (Figs. 6d and 6e). Further away from the fault, the borehole investigations revealed a decrease of approximately 1/m (Fig. 6e). At the 500 m depth, the fracture frequency was consistently high up to 60 m from the fault, and decreased at further distances (Fig. 7c). The fracture frequency near the fault was relatively high in the scan-line and borehole investigations, but this trend was less clear in gallery-wall mapping at the 500 m depth (Figs. 7d and 7e). In the scan-line and borehole investigations, the fracture frequency around the Small Fault at the 500 m depth was highest within 50 m of the Main Shaft Fault, and decreased further from the fault.

At both depths, the fractures were filled with calcites, hydrothermal minerals such as sericite and chlorite, and unconsolidated clayey fillings (clayey-type fillings). The details are given in Section 3-2. By “clayey-type filling,” I mean that the filling is

"clayey," not that the minerals are clay. Despite the abundance of calcite and hydrothermal minerals, clayey-type fillings were commonly observed within 75 m of the Main Shaft Fault (Fig. 6f). At the 500 m depth, the fracture fillings usually comprised calcite and hydrothermal minerals (Fig. 7f). Within 65 m of the Main Shaft Fault at this depth, more than 10% of the fracture fillings (with or without other minerals) were clayey-type (Fig. 7f).

WCFs comprised 11.4% of the detected fractures at the 300 m depth (191 of 1670 fractures; Fig. 6g) and 7.3% (146 of 2002 fractures) at the 500 m depth. At both depths, the trace lengths of the WCFs were longer than those of isolated, closed or sealed fractures (i.e., fractures without groundwater inflow) (Figs. 4a and 7b). At the 300 m depth, both the WCF frequencies and inflow rates were lower within 30 m from the Main Shaft Fault than beyond 30 m (Fig. 6g). The WCF percentage also increased with increasing distance from the fault. The hydraulic transmissivities of the rock mass were relatively low (less than 10^{-9} m^2/s) within 25 m from the fault at the 300 m depth (Fig. 6h), then increased up to 100 m from the fault. However, the transmissivities were lower in the individual fractures than in the rock mass beyond 100 m because the fracture frequency was higher between 25 and 100 m from the fault than beyond 100 m of the fault (Figs. 6e and 6h). At the 500 m depth, the inflow rates to the WCFs were relatively low within 50 m of the fault, and increased at larger distances from the fault (Fig. 7g). The hydraulic transmissivities were relatively low (less than 10^{-9} m^2/s) within 30 m of the fault at this depth (Fig. 7h) and increased at larger distances. However, the transmissivities never reached the high values in the individual fractures beyond 60 m of the fault, where the fracture frequency was lower than that around the fault (Figs. 7e and 7h). Around the Small Fault, the hydraulic transmissivity was 10^{-7} m^2/s. and was

lower in the individual fractures than at other locations. This result is attributed to the high fracture frequency around the Small Fault (over 10/m; see Figs. 7e and 7h). In addition, the transmissivity was relatively constant in the highly fractured zone, but varied widely in the less fractured zone at both gallery depths (Figs. 6h and 7h).

3-2. Relation between fracture trace length and fracture fillings

Figure 8a shows the frequency distribution of the fracture trace lengths. The fracture frequency was highest near the Main Shaft Fault, but relatively short trace fractures were commonly observed within 60 m of the Main Shaft Fault at the 500 m depth, abruptly decreasing thereafter (Fig. 8a). Conversely, the frequency of longer trace fractures was almost constant throughout the sample distance.

In the multivariate analysis, the trend of the fracture frequency distributions changed when the fracture trace length reached 4 m (Fig. 8c). The pattern of the normalized fracture frequencies also differed between long-traced (trace length $\geq$4 m) and short-traced (trace length < 4 m) fractures. The frequency of the short-traced fractures increased toward the Main Shaft Fault, whereas that of the long-traced fractures remained relatively constant (Fig. 8d).

Figure 9a shows the fracture fillings in the short- and long-traced fractures. The short-traced fractures tended to be filled only by hydrothermal minerals (sericite and/or chlorite) (Figs. 9b-1 and 9b-5), calcite (Figs. 9b-2 and 9b-3) or clayey-type fillings (Figs. 9b-6 and 10b). The long-traced fractures were filled by several minerals in a layered structure (Figs. 9b-2 and 9b-4) and characteristically exhibited large amounts of clayey-type fillings (Fig. 9a).

Polarizing optical microscopy observations revealed four types of calcite in the fracture fillings. Calcite I is anhedral and co-exists with hydrothermal minerals, sometimes forming a layered structure with those minerals (Fig. 9b-2; Ishibashi et al., 2014). Calcite II exists as spheres with radii of 0.1–0.2 mm (Fig. 9b-3; Ishibashi et al., 2014). Calcite III forms euhedral rhombohedra with a grain size of 0.5–1.0 mm, and is slightly elongated in the *c*-axis direction (Fig. 9b-3; Ishibashi et al., 2014). Calcite IV comprises fine-grained calcite and fragments of other minerals such as quartz, feldspar, and smectite (Fig. 9b-4). The $\delta^{18}O_{SMOW}$ of calcite I varied from −12.45‰ to −9.13‰ in calcite I, and from 20.01‰ to 24.70‰ in calcite II (Table 3). Meanwhile, the $\delta^{13}C_{PDB}$ ranged from −25.08‰ to −4.14‰ in calcite II and from −7.27‰ to −4.28‰ in calcite III (Table 3). In calcite IV, the $\delta^{18}O_{SMOW}$ and $\delta^{13}C_{PDB}$ ranged from 17.01‰ to 23.06‰ and from 16.55‰ to −9.22‰, respectively (Table 3). These calcites were sometimes layered with other calcite forms (Fig. 9b-4). Chloritized biotite and sericitized plagioclase was observed in the alteration haloes near fractures filled by calcite I, but not in haloes near fractures filled by calcite II and III. Fragments of quartz and feldspar were found in both hydrothermal minerals (Fig. 9b-5) and clayey-type fillings (Figs. 9b-6 and 10b).

The composition of the clayey-type fillings was confirmed by XRD analysis and microscopic observations. The investigations revealed smectite, calcite, and fragments of quartz, K-feldspar, plagioclase, and chlorite (Figs. 9b-6 and 10). This type of fracture filling is visible to the naked eye and also appears on the microscopic scale (microcracks; Figs. 9b-6 and 10b). The microcracks filled by clayey-type fillings exhibited no sheared structure (Fig. 10b), but imbrication-like fabric consisting of orientated fragments was recognized in the fillings themselves (Fig. 10b-2). The mineral

fragments in these fillings were larger in the central part than near the wall rock (Fig. 10b-3). The $\delta^{18}O_{SMOW}$ of the calcite in clayey-type fillings (calcite IV) ranged from 17.01‰ to 23.06‰ (Table 3).

Chapter 4: Discussion

4-1. Fracture formation and development, including the effect of faulting

As shown in the gallery-wall mapping results (Figs. 6c and 7c), the fracture frequencies increased toward the Main Shaft Fault. Particularly at 500 m below ground level, the fracture frequencies were clearly higher within 60 m of the Main Shaft Fault than at further distances (Fig. 7c). Similarly, at 300 m below ground level, the fracture frequency gradually decreased with increasing distance from the Main Shaft Fault (Fig. 6c). The zone of high fracture frequency was dominated by short-traced fractures (Figs. 6d and 7c; Table 4). The frequency of long-traced fractures was almost constant throughout the study area (Figs. 8a and 8d). A similar trend was observed in surface investigations of the Atera Fault, a major active fault in the northeastern part of the Chubu area, central Japan (Yoshida et al., 2014), and in the Äspö Hard Rock Laboratory in southeast Sweden (Bossart et al., 2001). The fracture orientation in the highly fractured zone was similar to that of the Main Shaft Fault at both depths (300 m and 500 m; see Figs. 6a, 6b and 7a, 7b). This suggests that the highly fractured zone is a mechanical damage zone associated with fault activity. Therefore, the short-traced fractures in the damage zone are considered to directly result from fault activities of the Main Shaft Fault.

Hydrothermal minerals such as chlorite and sericite were formed soon after brittle deformation (Nishimoto et al., 2008; Ishibashi et al., 2014). The fillings in the long-traced fractures include hydrothermal minerals (Fig. 9a), indicating that these fractures formed during the early cooling stage of the Toki granite. Yoshida et al. (2005,

2013b) showed that brittle tensile fractures (background fractures) form shortly after the temperature decreases to the ductile–brittle transition of granitic rocks. The formation of background fractures can be understood by Kakkonda granite, 0.34–0.07 Ma determined the K–Ar age of, hornblende, biotite, and K-feldspar (Kanisawa et al., 1994). The Kakkonda granite is still cooling from its high-temperature past; its current temperature is approximately 600 °C at 3000 m underground (Muraoka et al., 1998; Sasaki et al., 2003). No fractures were observed in the Kakkonda granite at depths below 3000 m (Matsushima and Okubo, 2003; Sasaki et al., 2003), however, surrounding background fractures and hydrothermal alterations were detected in the shallower part of the pluton (above approximately 3000 m). The temperature at this depth (300 °C–370 °C) has been suggested as the brittle–ductile transition (Matsushima and Okubo, 2003; Sasaki et al., 2003). Previous studies have shown that background fracture densities of different ages (1–120 Ma) are almost constant in post-formed Japanese plutons. This phenomenon is related to cooling of the plutonic rocks (Yoshida et al., 2005, 2013b, 2014). The frequency of the long-traced fractures was almost constant in the present study (Figs. 8a and 8d), implying a correspondence between these fractures and the background fractures formed before faulting.

The fracture frequencies were low in borehole investigations conducted at 300 m below ground level. Typically, they were reducing from 3/m to 1/m at distances beyond 100 m of the Main Shaft Fault (Fig. 6e and Table 4). This implies that at 300 m depth, the fractures were caused by faulting within 100 m of the fault. Therefore, the damage zone at this depth extends only to 100 m from the Main Shaft Fault.

The width of a mechanical damage zone (W_{dz}) caused by faulting is related to the length of the fault (L) as follows (Vermilye and Scholz, 1998):

$W_{dz} = 0.016*L.$ (2)

The maximum displacement of the fault (d) is also a function of the fault length (Cowie and Scholz, 1992):

$d = L^{1.5}/200.$ (3)

Moreover, field observations have revealed the following correlation between the width of a fault gouge (W_g) and the displacement of the fault (Scholz, 1987):

$W_g = 10^{-2}*d.$ (4)

From the fault gouge width, the damage zone widths at depths of 300 m and 500 m were estimated as approximately 96 and 67 m, respectively, along the Main Shaft Fault, and as approximately 11 m along the Small Fault. These widths are consistent with the damage zone widths estimated from the fracture frequencies based on geological investigations in the gallery. Yoshida et al. (2009) also confirmed that Eq. (2) estimates the scale of the damage zone in the Atera Fault. However, one-dimensional investigations of boreholes and scan-lines (Figs. 6d, 6e and 7d, 7e) cannot easily reveal the extent of a damage zone. The probability of intersection between fractures and boreholes (one-dimensional investigations) depends on factors such as the fracture frequency, fracture orientation with respect to the borehole, fracture length, relative position, borehole length, and borehole diameter (Martel, 1999). One-dimensional investigations tend to underestimate the fracture frequency because the chance of intersecting a borehole or scan line is higher for larger fractures than for smaller fractures (Ohnishi and Kagimoto, 1988; Martel, 1999). Therefore, the above equations are useful for estimating the scale of a damage zone along a fault.

4-2. Fracture filling process

At depths of 300 m and 500 m in the present study, the fracture fillings comprised sericite, chlorite, calcite, and smectite. Sericite and chlorite are common minerals in hydrothermally altered granitic rocks (Hedenquist, 1996; Nishimoto et al., 2008; Utada et al., 2003; Nishimoto and Yoshida, 2010). Sericitized plagioclase and chloritized biotite are characteristically observed in the vicinity (centimeters to decimeters) of fractures filled with sericite and chlorite, respectively. Occasionally, these minerals co-exist with quartz and feldspar fragments in the fractures (Fig. 9b-5). Such co-existence was previously reported by J'ebrak et al. (1997), Branquet et al. (1999), and Fujii (2000) and was attributed to high-pressure pore water formed via fluidization, which could enter the fractures by hydrothermal fluid and/or fault movement.

Calcite I commonly co-exists with sericite and exhibits a layered structure in fractures accompanying alteration halos (Figs. 9b-1 and 9b-2). This suggests an association between the hydrothermal origin of calcite I and the seritization of anorthite (Hamasaki et al., 1999). According to its O-isotopic composition ($\delta^{18}O_{SMOW}$ = 9.13‰–12.45‰), calcite I was precipitated in high-temperature fluid (approximately 150 °C–200 °C) (O'Neil et al, 1969; Iwatsuki et al, 2002). In addition, its occurrence is similar to the calcite formed in hydrothermal fluids described in previous studies (Nishimoto et al., 2008; Nishimoto and Yoshida, 2010; Ishibashi et al., 2014). Therefore, I conclude that calcite I precipitated in hydrothermal fluid at the study site.

Calcite II and III were observed only in fractures without clear alteration haloes. The euhedral crystals of Calcite III are slightly elongated parallel to the *c*-axis (Fig. 9b-3). The morphology of calcite depends on the groundwater condition (Folk, 1974; Iwatsuki

et al., 2002; Mizuno et al., 2010). The $\delta^{18}O_{SMOW}$ values of calcite II and III (approximately 20‰) indicate that both calcites formed in lower temperature fluid than calcite I (O'Neil et al, 1969; Iwatsuki et al., 2002). Ishibashi et al. (2014) suggested that the calcite III collected at the 300 m depth was precipitated from groundwater during the deposition of the Mizunami Group. The average $\delta^{13}C_{PDB}$ of calcite II and calcite III was approximately −12.65‰ and −5.39‰, respectively. In the marine and lacaustrine sedimentary rocks that unconformably cover the Toki granite, Shikazono and Utada (1997) reported calcite $\delta^{13}C_{PDB}$ values of −11‰ to +3‰ and −19‰ to −6‰, respectively. Iwatsuki et al. (2000) demonstrated the precipitation of calcite with near-zero $\delta^{13}C_{PDB}$ in marine water. These results suggest that calcite II and III originated from lacustrine and marine sources, respectively.

The clayey-type fillings were mainly observed in the extension joints and were composed of smectite co-existing with fragments of calcite IV, quartz and feldspar (Figs. 9b-6 and 10). Fractures filled with hydrothermal mineral fragments similarly occurred in the extension joints (Fig. 9b-5). Smectite is formed either in hydrothermal fluids or by interaction between sericite and relatively low-temperature groundwater (Taboada and Garcia, 1999; Meideno and Alistair, 1996; Yoshida et al., 2008; Nishimoto and Yoshida, 2010). Based on O-isotopic analysis, Yoshida et al. (2013b) inferred that the calcite in clayey-type fillings at the 300 m depth had precipitated in groundwater at approximately 30 °C. The $\delta^{18}O_{SMOW}$ values of calcite IV (approximately 17.01‰–23.06‰) were similar to those of calcite II and III, which also precipitated in relatively low-temperature fluid, or were intermediate between calcite I and calcites II and III. Calcite IV probably formed prior to smectite. Moreover, once the hydrothermal fluids had cooled to a relatively low-temperature, they failed to penetrate the Toki granite

(Yamasaki et al., 2013; Ishibashi et al., 2014). These results indicate that the smectite in clayey-type fillings formed under relatively low-temperature conditions. The imbrication-like structure of the clayey-type filling (Fig. 10b-2) implicates fluid flow. The uneven distribution of the fragments (Fig. 10b-3) can be attributed to frictional forces between the fragments, which would reduce the flow velocity near the fracture surface. This further supports that the clayey-type fillings formed by injection of fragments with smectite. Clayey-type fillings were mainly observed in the damage zones of the Main Shaft Fault and the Small Fault (Figs. 6f and 7f; Table 4). The present Main Shaft Fault were formed with the multiple reactivations occurring there (Tagami et al., 2012). The clayey-type filling proceeded first by the formation of smectite (an alteration product of low-temperature water–rock interactions), followed by the injection with high-pressure pore water due to fault activity.

4-3. Characteristics of WCF

Generally, fault damage zones are more permeable than fractured host rocks (Chester et al., 1993; JNC, 2000a; Faulkner et al., 2010). The high permeability of faults has been also confirmed at other underground facilities (Keusen et al., 1989; Nagra, 1994; Mazurek et al., 2003; SKB, 2006a, b), although, the permeability of the fractures in the damage zone around the Main Shaft Fault was low despite the fracture network development (Figs. 6 and 7; Table 4). The short-traced fractures have lost their WCF character, as they are sealed by minerals formed in a single type of groundwater (hydrothermal fluid or low temperature groundwater; Fig. 11). In the past, these fractures admitted groundwater through their open spaces. Most of the long-traced

fractures (background fractures) in the damage zone have remained as WCFs despite being filled with several minerals formed by different types of groundwater (Fig. 11a). The WCFs in the host rock are characteristically filled with calcite (Fig. 11b). The trace length distributions confirm that the relatively longer traced fractures (background fractures) act as WCFs, especially in the host rock (Fig. 12). Yuguchi et al. (2012) showed that background fracture distributions are controlled by local cooling rates. The fracture trace-length distributions in the underground environments of the Japanese islands have been determined in previous studies. Larger fractures are known to develop in older plutonic rocks (Fig. 13; Kawano and Ueda, 1995; Saitou et al., 1997, 1999; Ohtsu et al., 2001), and fractures are expanded by stress release during the uplifting of granitic rock (Fujii and Hori, 2002; Ishibashi et al., 2014). The background fractures exhibited the following characteristics: a) their distribution reflects the local differences in cooling rates after solidification; b) their density has remained almost constant since they were formed after the temperature had decreased through the ductile–brittle transition (approximately 300 °C–370 °C); c) they can potentially expand after their formation. From these results, I infer that background fractures in host rock develop through four steps: In Step A, the background fractures are generated under the stress associated with different local cooling rates of the granitic rock at sub-solidus temperatures (Yuguchi et al., 2012); in Step B, the background fractures form and the hydrothermal minerals (including calcite I) are precipitated out; in Step C, the background fractures are developed by uplifting of the granitic rock and calcite II precipitates due to infiltration of meteoric water; finally, calcite III precipitates due to penetration of paleo-seawater in Step D (Fig. 14). Thus, the long-traced fractures (background fractures) are likely to have persisted as WCFs to the present day

(long-term WCFs).

4-4. Long-term behavior of WCF related to faulting

From the above considerations, I infer that the fault-related hydrogeological structures in an active orogenic field develop in three stages: formation of the background fractures (Stage I), faulting and consequent formation of a damage zone along the fault (Stage II), and formation of fillings that eventually seal the fractures (Stage III) (Fig. 14).

4-4-1. Stage I: Formation of background fractures

In Stage I, the granitic rocks cool to below the ductile–brittle transition temperature (300 °C–370 °C), and subsequently develop background fractures (these have persisted as relatively longer fractures in the present rock). Most of these fractures were formed under brittle deformation conditions prior to fault development. The hydraulic transmissivity of granitic rock is largely controlled by the heterogeneity of the fracture distributions (Fig. 14). Hydrothermal circulation then deposited hydrothermal minerals (sericite, chlorite, and calcite I) in the background fractures, causing partial sealing.

4-4-2. Stage II: Faulting and formation of damage zone along the fault

In Stage II, the fault develops smaller fractures that form a fracture network. This fault activity leads to a damage zone with increased hydraulic transmissivity that

selectively admits groundwater (hydrothermal fluid and relative low temperature water) (Fig. 14). This process can explain the relation between the damage zone and permeability (Faulkner et al., 2010).

4-4-3. Stage III: Formation of fillings and sealing of the fractures

In Stage III, the smaller fractures formed by faulting are sealed by secondary minerals. The longer fractures (background fractures) also become filled by several minerals as various types of groundwater penetrate the damage zone and interact with the rock (Fig. 14). Once the pluton cools, the fault is reactivated and the shorter and longer (background) fractures of the damage zone become infiltrated with clayey-type fillings, reducing their hydraulic transmissivities. Several reports (Keusen et al., 1989; Mazurek et al., 2003; Yoshida et al., 2014) have suggested that fault reactivation can form gouges and breccias in previously deformed rocks (such as mylonites and cataclasites). Thus, the second and third stages have probably repeated several times. Consequently, the WCF content in the study area has reduced to approximately 10% (that is, almost 90% of the traceable fractures have lost their WCF functionality through sealing by fillings).

The predominance of clayey-type fillings is responsible for the low hydraulic transmissivity of the fractures in the damage zone. These minerals occupy even the microcracks and coats on the fracture surface (Figs. 9b-6 and 10b). Similar clayey-type fillings are observed in unsealed fractures at Kamaishi Mine in the northern part of Honshu (Tohoku area), and at the LPG storage facility located under the Seto Inland Sea in western Japan (JNC, 1999; Maejima and Nakajima, 2010). However, clayey-type

fillings are apparently absent in the tension cracks in stable continental rock (Yoshida, 2012). It seems that such fillings are a unique feature of active orogenic fields such as the Japanese islands.

The results indicate that faulting and reactivation in the active orogenic field of Japan has decreased the hydraulic permeability by sealing the WCFs in the damage zone.

Chapter 5: Conclusion

This study elucidated the distributions of fractures, fracture fillings, and hydraulic transmissivities in and around the damage zone along a fault identified in the granitic host rock distributed in the Toki area of central Japan. The aim was to relate the formation and sealing process to the groundwater flow in the underground environment.

The hydrogeological structures related to fracturing and faulting in the granitic rock distributed through an active orogenic field develop in three stages. The first stage forms the background fractures that act as long-term WCFs; the second stage forms the damage zone by faulting activity (the formation of relatively small fractures increases the hydraulic transmissivity in the damage zone, forming temporary WCFs); in the third stage, the fractures are penetrated by groundwater. The resulting mineral deposition effectively seals the WCFs in the rock body. Meanwhile, the long-term WCFs in the damage zone become characteristically filled with unconsolidated clayey-type fillings, which behave as a natural grout that reduces their hydraulic permeability. At present, nearly 90% of the traceable fractures are sealed by fillings and have lost their WCF functionality.

In conclusion, the reactivation of faults in underground environments can potentially decrease the hydraulic permeability of fractures by sealing the WCFs in the damage zone (Fig. 15). This process is favorable for long-term storage and is unique to active orogenic fields.

Acknowledgments

I would like to thank everybody who has helped and inspired me during my doctoral study. I especially want to thank my advisor, Professor H. Yoshida, for his guidance during my research. I thank Professors M. Takeuchi and K. Tsukada of Nagoya University, Dr. T. Yuguchi of Yamagata University, and Dr. S. Nishimoto of Nagoya City Science Museum for valuable discussion. Researchers at the Tono Geoscience Center of the Japan Atomic Energy Agency are acknowledged for their assistance and discussion during this study.

References

Aaltonen, I., Engström, J., Front, K., Gehör, S., Kosunen, P., Käuki, A., Mattila, J., Paananen, M., Paulamäki, S., 2016. Geology of Olkiluoto, POSIVA 2016-16.

Alexander, B., Shaun, F., Blomqvist, R., Pasi, N., 2000. Assessing the past thermal and chemical history of fluids in crystalline rock by combining fluid inclusion and isotopic investigations of fracture calcite. Applied Geochemistry 15, 1417-1437.

Alexander, B., Shaun, F., Blomqvist, R., Pasi, N., 2000. Assessing the past thermal and chemical history of fluids in crystalline rock by combining fluid inclusion and isotopic investigations of fracture calcite. Applied Geochemistry 15, 1417-1437.

Allen, C.J., Simmons, G.R., 1996. Canada's nuclear fuel waste management program: The environmental assessment of the disposal concept. Geological Problems in Radioactive Waste Isolation, Second Worldwide Review, 39-48.

Blyth, A., Frape, S., Blomqvist, R., Nissinen, P., 2000. Assessing the past thermal and chemical history of fluids in crystalline rock by combining fluid inclusion and isotope investigations of fracture calcite. Applied Geochemistry 13, 1417-1437.

Bossart, P., Hermanson, J., Mazurek, M., 2001. Äspö Hard Rock Laboratory: Analysis of fracture networks based on the integration of structural and hydrogeological observations on different scales. SKB TR-01-21.

Branquet, Y., Cheilletz, A., Giuliani, G., Laumonier, B., Blanco, O., 1999. Fluidized hydrothermal breccia in dilatant faults during thrusting: The Colombian emerald deposits. Geological Society, London, Special Publications 155, 183-195.

Chester, F.M., Evans, J.P., Biegel, R.L., 1993. Internal structure and weakening mechanisms of the San Andreas Fault. Journal of Geophysical Research 98,

771-786.

Committee for Geological Stability Research, 2011. Geological Leaflet 4, Japanese island-arc and geosphere stability. Geological Society of Japan. (in Japanese)

Cowie, P.A., Scholz, C.H., 1992. Displacement-length scaling relationship for faults: Data synthesis and discussion. Journal of Structural Geology 14, 1149-1156.

Degnan, P., Bath, A. (eds.), 2005. PADAMOT: Project overview report. PADAMOT Project Technical Report. United Kingdom Nirex Limited, Harwell, 85p.

Faulkner, D.R., Jackson, C.A.L., Lunn, R.J., Schlische, R.W., Shipton, Z.K., Wibberley, C.A.J., Withjack, M.O., 2010. A review of recent developments concerning the structure, mechanics and fluid flow properties of fault zones. Journal of Structural Geology 32, 1557-1575.

Folk, R.L., 1974. The natural history of crystalline calcium carbonate: Effect of magnesium content and salinity. Journal of Sedimentary Petrology 44, 40-53.

Follin, S., Levén, J., Hartley, L., Jaclson, P., Joyce, S., Roberts, D., Swift, B., 2007. Hydrogeological characterization and modelling of deformation zones and fracture domains, Forsmark modelling stage 2.2. SKB TR-07-48.

Follin, S., 2008. Bedrock hydrogeology Forsmark Site descriptive modelling, SDM-Site Forsmark. SKB TR-08-95.

Fujii, Y., 2000. Fracture analysis of the Toki Granite in the Tono district, central Japan. Journal of the Geological Society of Japan 106, 249-263. (in Japanese with English abstract)

Fujii, Y., Hori, S., 2002, Chronological analysis of fracture in Granitic rock, Annual report of Fukada Geological Institute 3, 59-77. (in Japanese with English abstract)

Grink, P., 1993. OECD/NEA International Stripa Project overview, Vol.II: Natural

Barrier. SKB.

Hartley, L., Hoek, J., Swan, D., Appleyard, P., Baxter, S., Roberts, D., Simpson, T., 2013. Hydrogeological modeling for assessment of radionuclide release scenarios for the repository system 2012, POSIVA Working Report 2012-42.

Hasaki, S., Tsukimura, K., Fujimoto, K., Ikeda, R., Omura, K., 1999. Alteration and calcite formation in the granitic rocks, Asio area, central Japan. Bulletin of the Geological Survey of Japan 50, 499-508. (in Japanese with English abstract)

Hedenquist, J.W., Izawa, E., Arribas, A., White N.C., 1996. Epithermal gold deposits: Styles, characteristics and exploration. Resource Geology: Special Publication 1.

IAEA, 1983a. Criteria for underground disposal of radioactive waste. IAEA Safety Series Report No. 60. International Atomic Energy Agency Vienna, Austria.

IAEA, 1983b. Advisory group meeting on stable isotope reference samples for geochemical and hydrological investigations. IAEA Vienna.

Ijiri, Y., Sawada, A., Akahori, K., 1999. Fracture characteristics in Japanese rock. JNC-TN8400 99-091. (in Japanese with English abstract)

Ijiri Y., Sawada A., Sakamoto K., Uchida M., Ishiguro K., Umeki H., Ohnishi Y., 2001. Evaluation of scale effects on hydraulic characteristics of fractured rock using fracture network model. Journal of Japan Society of Civil Engineers 694, 179-194. (in Japanese with English abstract)

Ishibashi, M., Sasao, E., Kuboshima, K., Matsuioka, T., 2013. Development of geological models in the Mizunami Underground Research Laboratory Project; Updating results of “Shaft460 geological model” and “shaft500 geological model” in Phase 2. JAEA-Research 2013-019. (in Japanese with English abstract)

Ishibashi, M., Ando, T., Sasao, E., Yuguchi, T., Nishimoto, S., Yoshida, H., 2014.

Characterization of water conducting fracture and their long-term behavior in deep crystalline rock; A case study of the Toki granite. Journal of the Japan Society of Engineering Geology 55, 156-165. (in Japanese with English abstract)

Ishibashi, M., Yoshida, H., Sasao, E., Yuguchi, T., 2016. Long term behavior of hydrogeological structures associated with faulting; An Example from the deep crystalline rock in the Mizunami URL, Central Japan. Engineering Geology 208, 114-127.

Ishihara S., Chappell B., 2007. Chemical compositions of the late Cretaceous Ryoke granitoids of the Chubu District, central Japan – revisited. Bulletin of the Geological Survey of Japan 58, 323-350.

Itoigawa, J., 1974. Geology of the Mizunami district, central Japan. Bulletin of the Mizunami Fossil Museum 1, 9-42. (in Japanese)

Itoigawa, J., 1980. Geology of the Mizunami district, central Japan. Monograph of the Mizunami Fossil Museum 1, 1-50. (in Japanese)

Iwatsuki T., Satake H., Metcalfe R., Yoshida H. and Hama K., 2002. Isotopic and morphological features of fracture calcite from granitic rocks of the Tono area, Japan: A promising palaeohydrogeological tool. Applied Geochemistry 17, 1-50.

Jébrak, M., 1997. Hydrothermal breccias in vein-type ore deposits: A review of mechanisms, morphology and size distribution. Ore geology reviews 12, 111-134.

JNC (Japan Nuclear Cycle Development Institute), 1999. Proceedings of an International Workshop for the Kamaishi In-situ Experiments. JNC TN 7400 99-007.

JNC (Japan Nuclear Cycle Development Institute), 2000a. H12: Project to establish the scientific and technical basis for HLW disposal in Japan. Project Overview Report.

JNC TN 1410 2000-001.

JNC (Japan Nuclear Cycle Development Institute), 2000b. Regional Hydrogeological Study Project Result from 1992-1999. JNC TN 7400 2003-007.

JNC (Japan Nuclear Cycle Development Institute), 2002. Master plan of the Mizunami Underground Research Laboratory Project. JNC TN7410 2003-001.

Kanisawa, S., Doi, N., Kato, O., Ishikawa, K., 1994. Quaternary Kakkonda Granite underlying the Kakkonda Geothermal Field, Northeast Japan. Journal of Mineralogy, Petrology and Economic Geology 89, 390-407. (in Japanese with English abstract)

Kawamoto, K., Kuboshima, K., Ishibashi, M., Tsuruta, T., Sasao, E., Ikeda, K., Mikake, S., Hara, I., Yamamoto, M., 2012. Mizunami Underground Research Laboratory Project, Compilation of results of geological investigation at the shafts and research galleries. JAEA-Data/Code 2012-009. (in Japanese with English abstract)

Kawamoto, K., Kuboshima, K., Ishibashi, M., Tsuruta, T., Sasao, E., Ikeda, K., Mikake, S., Hara, I., Yamamoto, M., 2013. Mizunami Underground Research Laboratory Project; Compilation of results of geological investigation at the shafts and research galleries from the depth of 300m to 500m. JAEA-Data/Code 2012-025. (in Japanese with English abstract)

Kawamoto, K., Kuboshima, K., Murakami, H., Ishibashi, M., Sasao, E., 2014. Study on geology on the Mizunami Underground Research Laboratory Project; Geology and geological structure at the -500m stage. JAEA-Research 2014-021. (in Japanese with English abstract)

Kawano, Y., Ueda, Y., 1965. K-Ar dating on the igneous rocks in Japan (II) Granitic rocks in Kitakami massif. The Journal of the Japanese Association of Mineralogists,

Petrologists and Economic Geologists 53, 143-154. (in Japanese with English abstract)

Keusen, H.R., Ganguin, J. Schuler, P., Buletti, M., 1989. Grimsel Test Site: Geology. Nagra Technical Report NTB 87-14 E.

Kuboshima, K., Ishibashi, M., Sasao, E., Tsuruta, T., Tagami, M., Yuguchi, T., 2013. Study on geology on the Mizunami Underground Research Laboratory Project; Geology and geological structure from the surface to G.L.-300m. JAEA-Research 2012-037. (in Japanese with English abstract)

Kurihara A., Amano K., Liu C., Koike K., 2008. Characterization and tectonic significance of low-angle fracture distribution in the upper part of a granite body - new insight from the Toki granite around the Mizunami Underground Research Laboratory (MIU), central Japan. Journal of the Mining and Materials Processing Institute of Japan 124, 710-718. (in Japanese with English abstract)

Maejima, T., Nakajima, S., 2010. Hydrogeological modeling for groundwater management in underground LPG storage construction. Journal of Japanese Geotechnical Society 58, 12-15. (in Japanese)

Martel, S.J., 1999. Analysis of fracture orientation data from boreholes. Environmental & Engineering Geoscience 5, 213-233.

Matsushima, J., Okubo Y., 2003. Rheological implications of the strong seismic reflector in the Kakkonda geothermal field, Japan. Tectonophysics 371, 141-152.

Mazurek, M., Jakob, A., Bossart, P., 2003. Solute transport in crystalline rocks at Äspö—I: Geological basis and model calibration. Journal of Contaminant Hydrology 61, 157-174.

Meideno, Que., Alistair, R.A., 1996. Sericitization of plagioclase in the Rosses Granite

Complex, Co. Donegal, Ireland. Mineralogical Magazine 60, 927-936.

Mikake, S., Yoshida, H., Koide, K., Yanagisawa, K., Ogata, N., Maekawa, K., 2000. Methodology development for modeling heterogeneous conductivity fields for a sandstone type uranium deposit, central Japan. Engineering Geology 56, 185-195.

Mikake, S., Yamamoto, M., Ikeda, K., Sugihara, K., Takeuchi, S., Hayano A., Sato T., Takeda, S., Ishii Y., Ishida, H., Asai, H., Hara, M., Kuji, M., Minamide, K., Kuroda, H., Matsui, H., Tsuruta, T., Takeuchi, R., Saegusa, H., Matsuoka, T., Mizuno, T., Oyama, T., 2010. Studies on planning and conducting for reducing water inflow due to underground construction in crystalline rock. JAEA-Technology 2010-026. (in Japanese with English abstract)

Mizuno, T., Milodowski, A., Iwatsuki, T., 2010. Evaluation of the long-term evolution of the groundwater system in the Mizunami area, Japan. Proceedings of 13th International Conference on Environmental Remediation and Radioactive Waste Management (ICEM 2010) (CDROM), 9p.

Muraoka, H., Uchida, T., Sasada, M., Yagi, M., Akaku, K., Sasaki, M., Yasukawa, K., Miyazaki, S., Doi, N., Saito, K., Tanaka, S., 1998. Deep geothermal resources survey program: A link of igneous, metamorphic and hydrothermal processes in the well encountered 500°C at 3,729 m. Geothermics 27, 507-534.

Nagra, 1985. Grimsel Test Site: Overview and test programs. Nagra Technical Report NTB 85-46.

Nagra, 1994. Kristall in-I: Safety Assessment Report. Nagra Technical Report NTB 93-22.

Narasimham, T.N., 1982. Recent trends in hydrogeology. The Geological Society of America, Special Paper 189, 3-25.

Neretnieks, I., 1990. Solute transport in fractured rock: Applications to radioactive waste repositories. SKB Technical Report TR90-38.

Nishimoto, S., Ukai, E., Amano, K., Yoshida H., 2008. Alteration process in deep granitic rock - an example of Toki granite, central Japan. Journal of the Japan Society of Engineering Geology 49, 94-104. (in Japanese with English abstract)

Nishimoto, S., Yoshida, H., 2010. Hydrothermal alteration of deep fractured granite: Effect of dissolution and precipitation. Lithos 115, 153-162.

Nishimoto, S., Yoshida, H., Asahara, Y., Tsuruta, T., Ishibashi., M., Katsuta, N., 2014. Episyenite formation in the Toki granite, central Japan. Contributions to Mineralogy and Petrology 167, 960.

O'Neil, J.R., Clayton, R.N., Maeda, T.K., 1969. Oxygen isotope fractionation in divalent metal carbonates. Journal of Chemical Physics 51, 5547-5558.

Ohnishi, Y., Kagimoto, H., 1998. A method of evaluation for two- and three-dimensional discontinuity networks. Proceedings of the Japan Society of Civil Engineers, 29-38. (in Japanese with English abstract)

Ohtsu, H., Nishiyama, S., Tsuchiya, T., Nakai, R., Sawada, A., Yamada, N., Sakamoto, K., Uchida, M., 2001. Characteristics and modeling of fractures in Japanese rock mass (evaluation of confidence in fracture network model). JNC TY8400 2001-004. (in Japanese with English abstract)

Piggott, A.R., 1997. Fractal relations for the diameter and trace length of disc-shaped fractures. Journal of Geophysical Research 102, 18121-18125.

Power Reactor and Nuclear Fuel Development Corporation (PNC), 1994. Uranium resources in Japan. PNC-TN7420 94-006. (in Japanese)

Raymond, M., Svensk, K.A.B., 2004. Statistical analysis of fracture data, adapted for

modelling Discrete Fracture Networks-Version 2. SKB Report R-04-66.

Saegusa, H., Onoe, H., Ishibashi, M., Tanaka, T., Abumi, K., Hashimoto, S., Bruines, P., 2015. Study for development of the methodology for multi-scale hydrogeological modeling taking into account hydraulic heterogeneity caused by fracture network. JAEA-Research 2015-011. (in Japanese with English abstract)

Saito, S., Morooka, K., Ikeda, N., Sugiyama, K., Tomiyama, S., Kawakami, K, 1997. Basic study for the modeling of mass transfer path in near field geological environment (IV). PNC-ZJ1211 97-002. (in Japanese with English abstract)

Saito, S., Sugiyama, K., Morooka, K., Ikeda, N., 1999. Basic study for the modeling of mass transfer path in near field geological environment (VI). JNC-TJ1400 99-014. (in Japanese with English abstract)

Sakai, T., Nohara, T., Ishibashi, M., 2016. Development of geological models in the Mizunami Underground Research Laboratory Project; Updating from “Shaft500 Geological Model” to “Stage500 Geological Model” in Phase II. JAEA-Research 2016-009. (in Japanese with English abstract)

Sasada, M., Sakaki, M., 2004. High-temperature granitoids at cooling stages from active geothermal systems including the Kakkonda granite. Chishitsu News 593, 49-58. (in Japanese)

Sasaki, M., Fujimoto, K., Sawaki, T., Tsukamoto, H., Kato, O., Komatsu, R., Doi, N., Sasada. M., 2003. Petrographic features of a high-temperature granite just newly solidified magma at the Kakkonda geothermal field, Japan. Journal of Volcanology and Geothermal Research 121, 247-269.

Sasao, E., Amano, K., Ota, K., 2005. Natural analogue study in the Tono uranium deposit - Quantitative estimation of uplift and subsidence, and vertical

displacement rate. Journal of Nuclear Fuel Cycle and Environment 11, 167-180. (in Japanese with English abstract)

Sasao E., Iwano H., Danhara T., 2006. Fission track ages of tuffaceous sandstone from the Toki Lignite-bearing Formation of the Mizunami Group in the Tono district, Gifu Prefecture, central Japan. Journal the Geological Society of Japan 112, 459-468. (in Japanese with English abstract)

Sasao, E., Yuguchi, T., Itoh, Y., Inoue, T., Ishibashi, M., 2015, Formative mechanism of inhomogeneous distribution of fractures, example of the Toki Granite, Central Japan, proceedings of 10th Asian Regional Conference of IAEG (2015), 1-6.

Sawada, A., Ijiri, Y., Skamoto, K., Watari, S., 1999. Nuclide migration analysis in fractured rock. JNC TN8400 99-093. (in Japanese with English abstract)

Sawada, A., Saegusa, H., Takeuchi, S., Sakamoto, K., Dershowitz, W.S., 2015. Äspö Task Force on modelling of groundwater flow and transport of solutes. Task 7– Groundwater flow and transport modelling of fracture system at regional, block, and single-fracture scale flow and transport, Olkiluoto, SKB P-13-46.

Scholtz, C.H., 1987. Wear and gouge formation in brittle faulting. Geology 15, 493-495.

Scholtz, C.H., Cowie, P.A., 1990. Determination of total strain from faulting using slip measurements. Nature 346, 837.

Shibata K., Ishihara S., 1979. Rb-Sr whole-rock and K-Ar mineral ages of granitic rocks in Japan. Geochemical Journal 13, 113-119.

Shikazono, N., Utada, M., 1997. Stable isotope geochemistry and diagenetic mineralization associated with the Tono sandstone-type uranium deposit in Japan. Mineralium Deposita 32, 596-606.

SKB, 1995. Feasibility study for siting of a deep repository within the Storuman

municipality. SKB Technical Report 95-08.

SKB, 2006a. Long-term safety for KBS-3 repositories at Forsmark and Laxemar - a first evaluation. Main Report of the SR-Can project, SKB Technical Report TR06-09.

SKB, 2006b. Data report for the safety assessment SR-Can, SKB Technical Report TR06-25.

SKB, 2008. Geological evolution, palaeoclimate and historical development of the Forsmark and Laxemar-Simpevarp areas: Site descriptive modelling SDM-Site. SKB R-08-19.

SKB, 2010. Fault Rock Zones Characterization–Final report TRUE-1 Continuation Project. SKB Technical Report TR10-36.

SKB, 2011. Long-term safety for the final repository for spent nuclear fuel at Forsmark Main report of the SR-Site project Volume I. SKB Technical Report TR11-01.

SKB, 2014. Safety analysis for SFR Long-term safety: Main report for the safety assessment SR-PSU. SKB Technical Report TR14-01.

Suzuki K., Adachi M., 1998. Denudation history of the high T/P Ryoke metamorphic belt, southwest Japan: Constraints from CHIME monazite ages of gneisses and granitoids. Journal of Metamorphic Geology 16, 27-37.

Taboada, T., Garcia, C., 1999. Smectite formation produced by weathering in a coarse granite saprolite in Galicia (NW Spain). Catena 35, 281-290.

Tagami, M., Yamada, Y., Yamashita, Y., Miyakawa, A., Matsuoka, T., Xue, Z., Tsuji, T., Tsuruta, T., Matsuoka, T., Amano, K., Hama, K., Sasao, E., 2013. Development of geological structure modeling technology based on regional tectonic process. JAEA-Research 2012-036. (in Japanese with English abstract)

Terzaghi, R., 1965. Sources of error in joint surveys. Geotechnique 15, 287-304.

Tsuruta, T., Tagami, M., Amano, K., Matsuoka, T., Kurihara, A.,Yamada, Y., Koike, K., 2013. Geological investigations for geological model of deep underground geoenvironment at the Mizunami Underground Research Laboratory (MIU). The Journal of the Geological Society of Japan 119, 59-74. (in Japanese with English abstract)

Turcotte, D.L., 1986. Fractals and fragmentation. Journal of Geophysical Research 91, 1921-1926.

Utada, M, 2003. Alteration of Rokko Granites mineralogical and magnetic susceptibility changes. Journal of Geography 112, 360-371. (in Japanese with English abstract)

Vermilye, J.M., Scholz, C.H, 1998. The process zone: A micro-structural view of fault growth. Journal of Geophysical Research 103, 12223-12237.

Witherspoon, P.A., 1979. Observations of a potential size effect in experimental determination of the hydraulic properties of fractures. Water Resources Research 15, 1142-1146.

Witherspoon, P.A., Gale, J.E., 1977. Mechanical and hydraulic properties of rocks related to induced seismicity. Engineering Geology 11, 23-55.

Yamasaki S., Umeda K., 2012. Cooling history of Cretaceous Toki granite in the eastern Sanyo Belt, central Japan. Japanese Magazine of Mineralogical and Petrological Sciences 41, 39-46. (in Japanese with English abstract)

Yamasaki, S., Zwingmann, H., Yamada, K., Tagami, T., Umeda K., 2013. Constraining the timing of brittle deformation and faulting in the Toki granite, central Japan. Chemical Geology 351, 168-174.

Yasue, K., Ishimaru, T., Kobori, K., Umeda, K., Nakatsuika, N., 2014. Subsurface geological mapping of the Japanese Islands. The Journal of the Geological Society

of Japan 120, XIII-XIV.

Yoshida, H., Aoki, K., Semba, T., Ota, K., Amano, K., Hama, K., Kawamura, M., Tsubota, K, 2000. Overview of the stability and barrier functions of the granitic geosphere at the Kamaishi Mine: Relevance to radioactive waste disposal in Japan. Engineering Geology 56, 151-162.

Yoshida, H., Sato, H., Semba, T., 2002. Evaluation of an investigation methodology for nuclide retardation by matrix diffusion. Journal of the Japan Society of Engineering Geology 43, 24-34. (in Japanese with English abstract)

Yoshida, H., Takeuchi, M., Metcalfe, R., 2005. Long-term stability of flow-path structure in crystalline rocks distributed in an orogenic belt, Japan. Engineering Geology 78, 275-284.

Yoshida, H., Nishimoto, S., Yamamoto, K., Katsuta, N., 2008. Alteration of subsurface granitic rock in Okayama Area, Japan. Journal of the Japan Society of Engineering Geology 49, 256-265. (in Japanese with English abstract)

Yoshida, H., Oshima, K., Yoshimura, K., Nagatomo, A., Nishimoto, S, 2009. Fracture characterization along the fault - A case study of ‘Damaged Zone’ analysis on Atera Fault, central Japan. Journal of the Japan Society of Engineering Geology 50, 16-28. (in Japanese with English abstract)

Yoshida, H., 2012. Fluid conducting fractures and their long-term behavior in crystalline rocks present understanding and future perspectives. Journal of Geography (Chigaku Zasshi) 121, 68-95. (in Japanese with English abstract)

Yoshida, H., Maejima, T., Nakajima, S., Nakamura, Y., Yoshida, S., 2013a. Features of fractures forming flow paths in granitic rock at an LPG storage site in the orogenic field of Japan. Engineering Geology 152, 77-86.

Yoshida, H., Metcalfe, R., Ishibashi, M., Minami, M., 2013b. Long-term stability of fracture systems and their behaviour as flow paths in uplifting granitic rocks from the Japanese orogenic field. Geofluids 13, 45-55.

Yoshida, H., Nagatomo, A., Oshima, A., Metcalfe, R, 2014. Geological characterization of the active Atera Fault in central Japan: Implications for defining fault exclusion criteria in crystalline rocks around radioactive waste repositories. Engineering Geology 177, 93-103.

Yuguchi, T., Amano, K., Tsuruta, T., Danhara, T., Nishiyama T., 2011. Theremochronology and the three-dimensional cooling pattern of granitic pluton: An example of the Toki granite, central Japan. Contributions to Mineralogy and Petrology 162, 1063-1077.

Yuguchi, T., Tagami, M., Tsuruta, T., Nishiyama, T., 2012. Three-dimensional fracture distribution in relation to local cooling in a granitic body: An example from the Toki granitic pluton, Central Japan. Engineering Geology 149-150, 35-46.

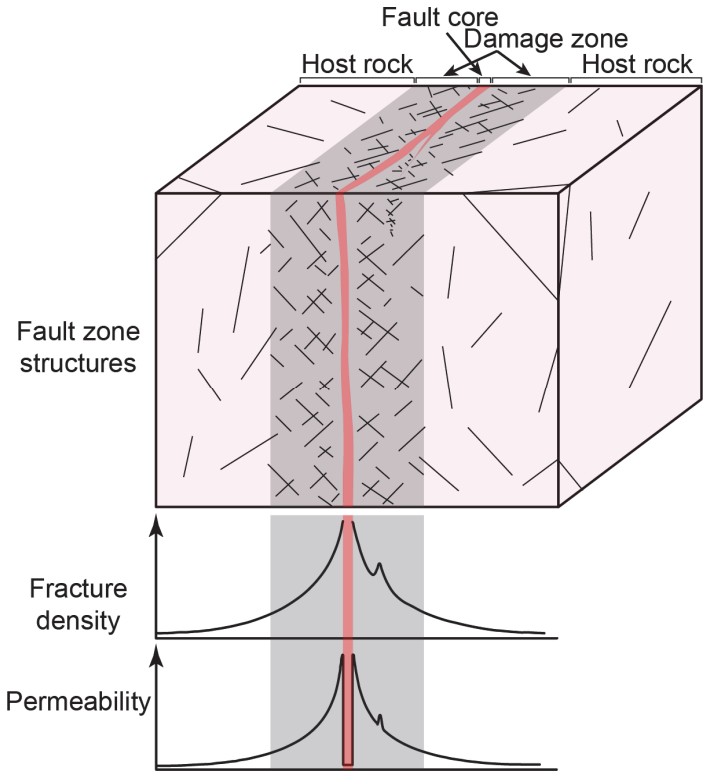

Fig. 1 Schematic of the physical property distributions (fracture density and permeability) in a typical fault damage zone. Modified from Faulkner et al. (2010).

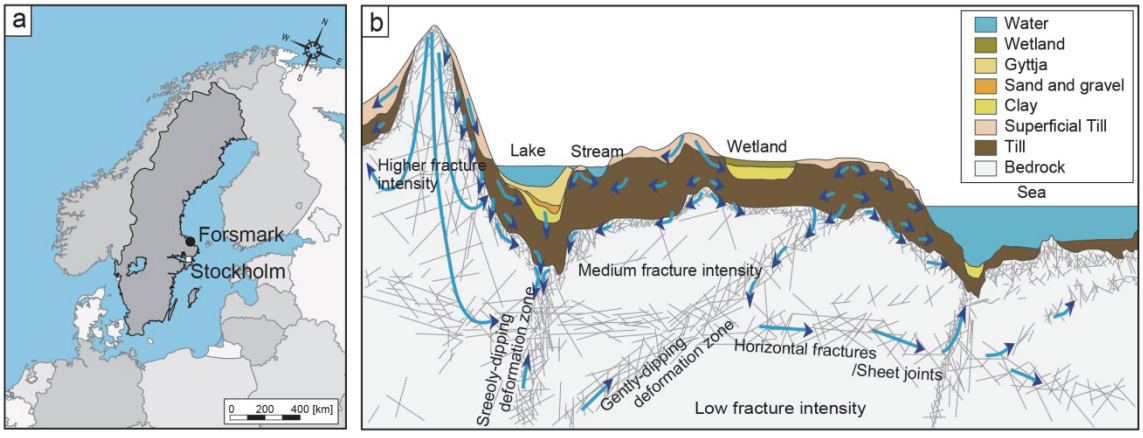

Fig. 2 (a) Location map of the Forsmark site in Sweden. (b) A conceptual hydrogeological model of the Forsmark vicinity. The low-angle fractured zone formed by deglaciation is regarded as an important hydrogeological structure. Modified from Follin et al. (2007).

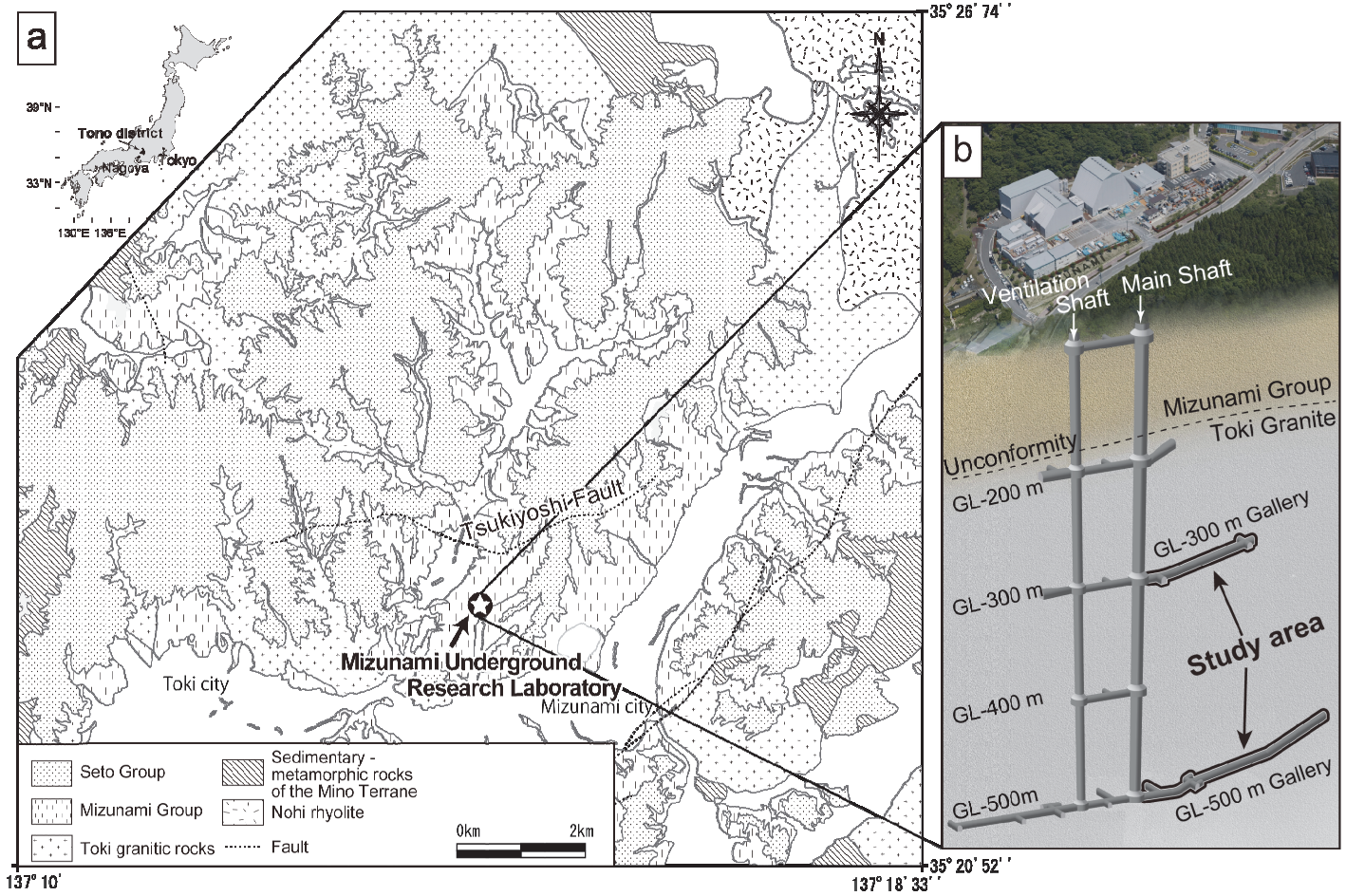

Fig. 3 Location map of the Mizunami Underground Research Laboratory (MIU) site, together with (a) a geological map of the site showing the distribution of the Toki granite (after PNC, 1994) and (b) a schematic of the MIU site showing the location of this study. Note that GL – means ground level minus.

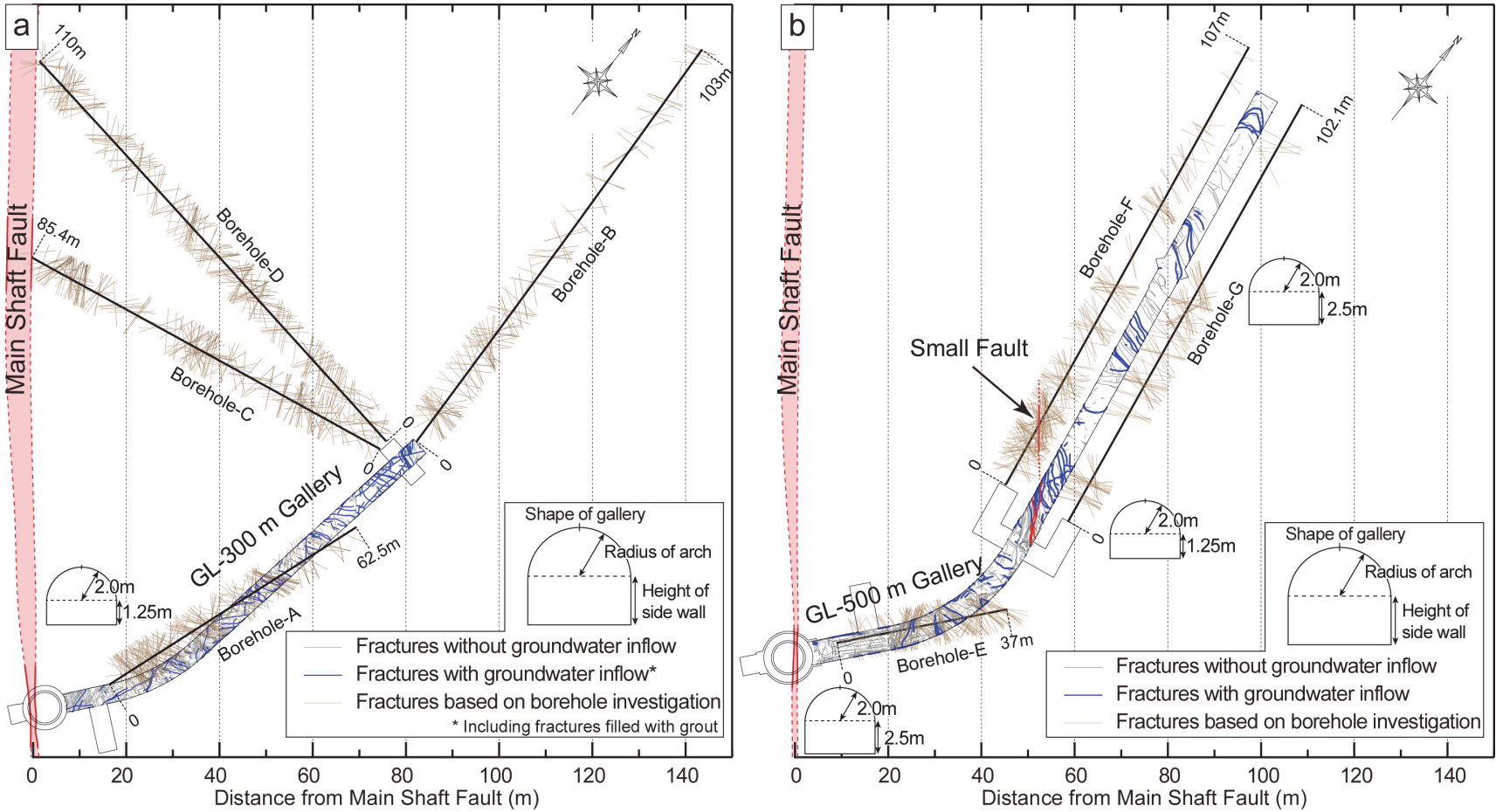

Fig. 4 Layout of galleries and boreholes, and the distribution of fractures and faults, based on borehole investigations and gallery wall mapping at (a) 300 m and (b) 500 m below ground level. (After Ishibashi et al., 2016).

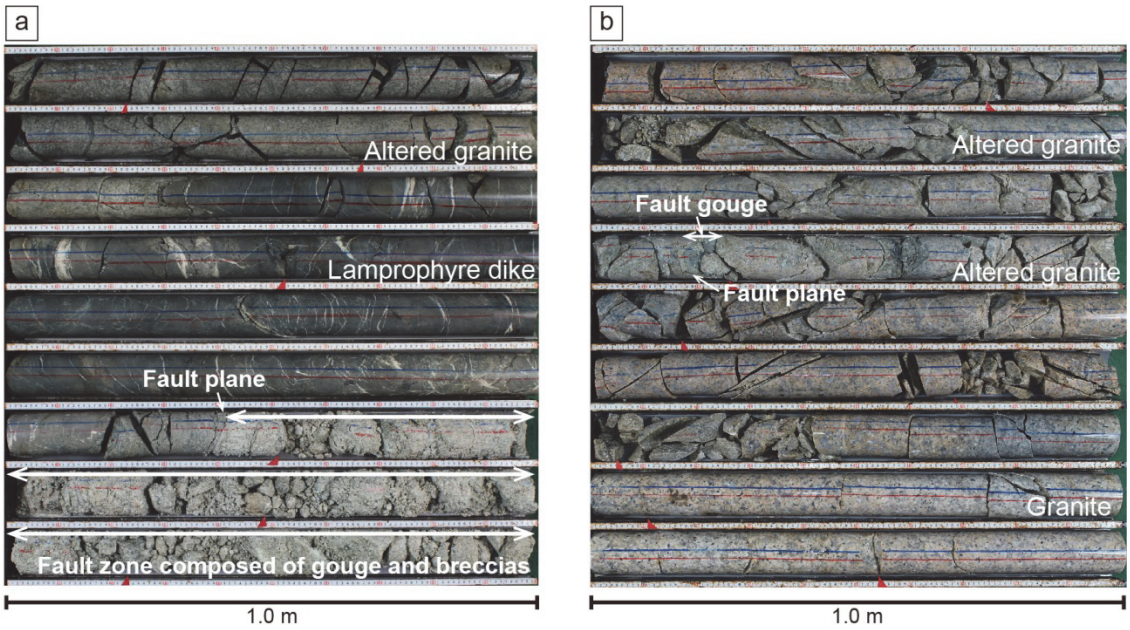

Fig. 5 Photographs of rock core samples showing the faults and adjacent wall rocks. (a) Major fault crossing the main shaft (Main Shaft Fault), with lamprophyre dike and strongly altered granite in borehole-C and (b) Small Fault, with altered granite at 500 m below ground level in borehole-F. (After Ishibashi et al., 2016).

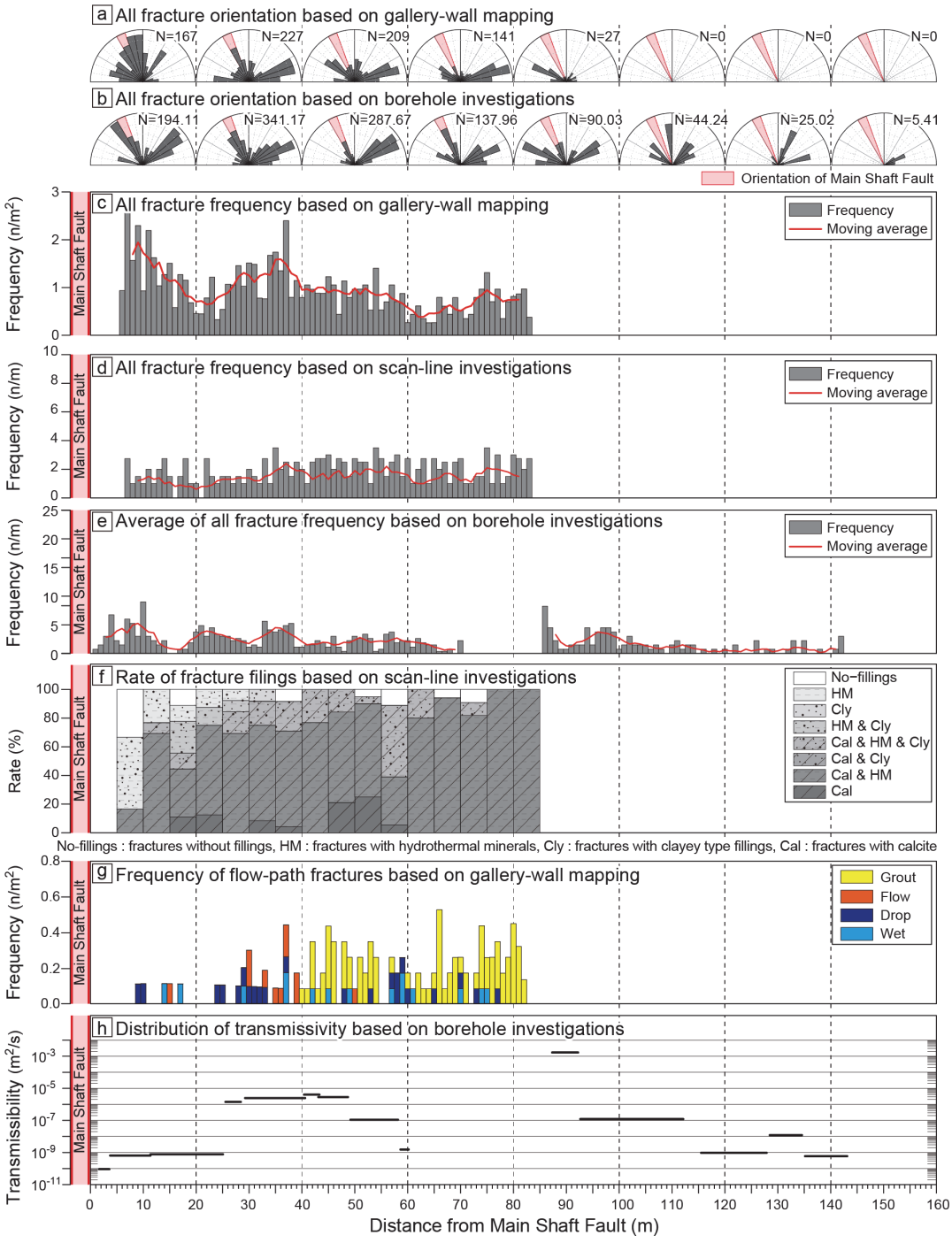

Fig. 6 (a, b) Distributions of fracture orientations, (c, d) all fracture frequencies based on geological investigations in the gallery, and (e) averaged fracture frequencies based on borehole investigations. (f) Fracture fillings and (g) water-conducting fractures (WCFs) based on investigations in the gallery, and (h) transmissivities around the Main Shaft Fault at 300 m below ground level. Modified from Ishibashi et al. (2016).

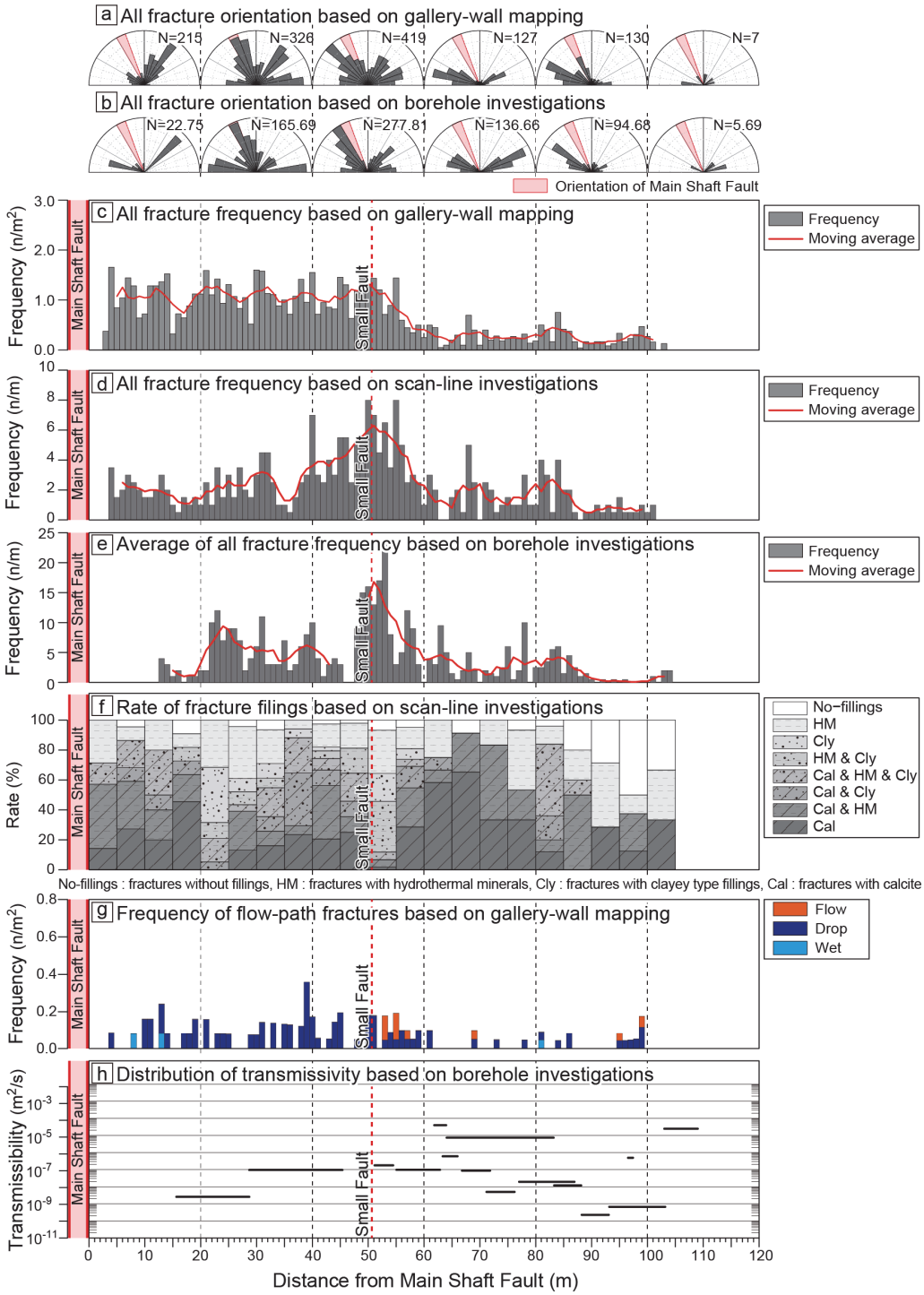

Fig. 7 (a, b) Distributions of fracture orientations, (c, d) all fracture frequencies based on geological investigations in the gallery, and (e) averaged fracture frequencies based on borehole investigations. (f) Fracture fillings and (g) WCFs based on investigations in the gallery, and (h) transmissivities around the MSF at 500 m below ground level. Modified from Ishibashi et al. (2016).

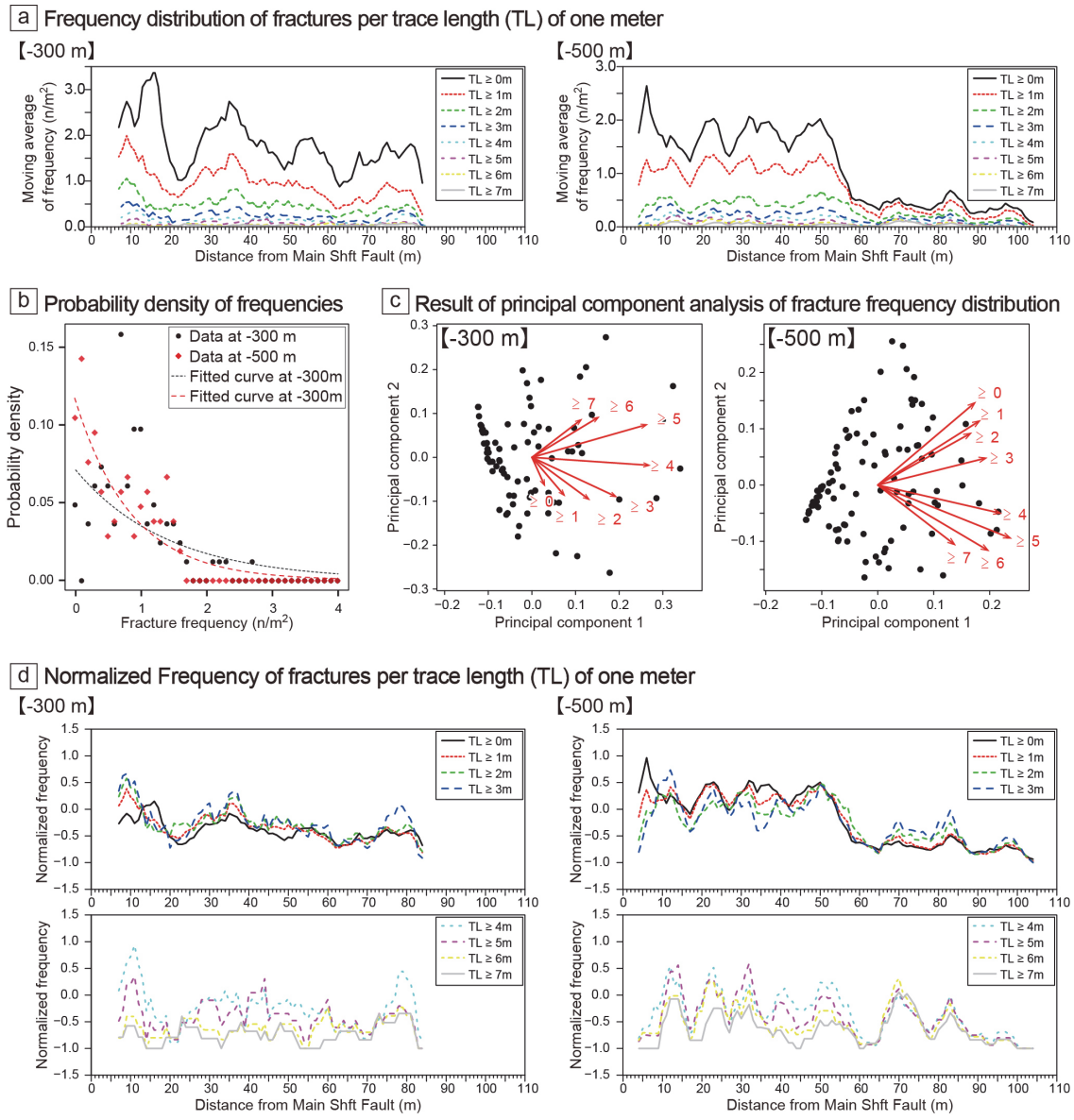

Fig. 8 (a) Frequency distributions of fracture trace lengths in 1-m intervals; (b) probability density of fracture frequencies (assumed as an exponential distribution); (c) biplot of principal component analysis based on the normalized frequency distribution of fractures; (d) distributions of the normalized frequencies per 1-m trace length of fractures with relatively short trace lengths (upper charts) and relatively long trace lengths (lower charts). After Ishibashi et al. (2016).

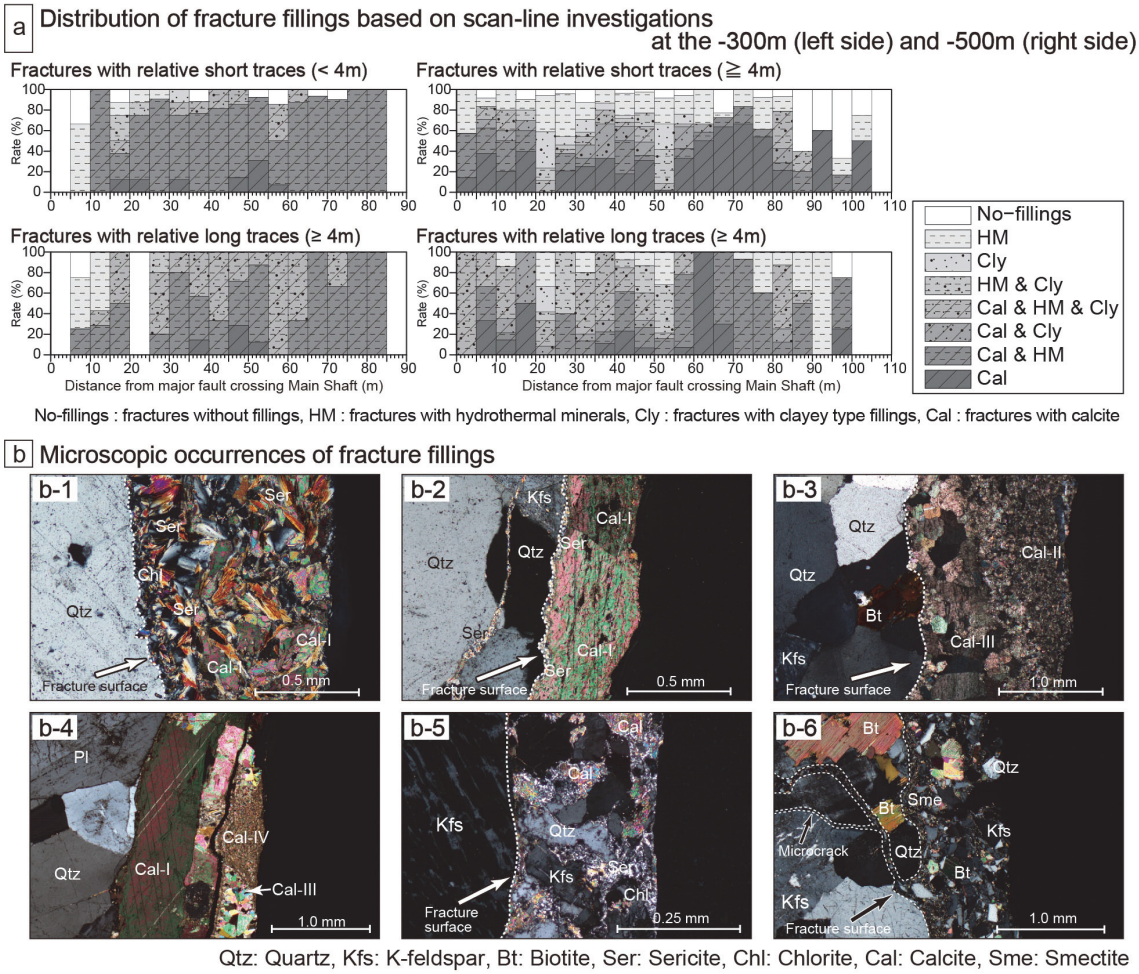

Fig. 9 (a) Relations between fracture fillings and trace lengths and (b) occurrences of fracture fillings. Modified from Ishibashi et al. (2016).

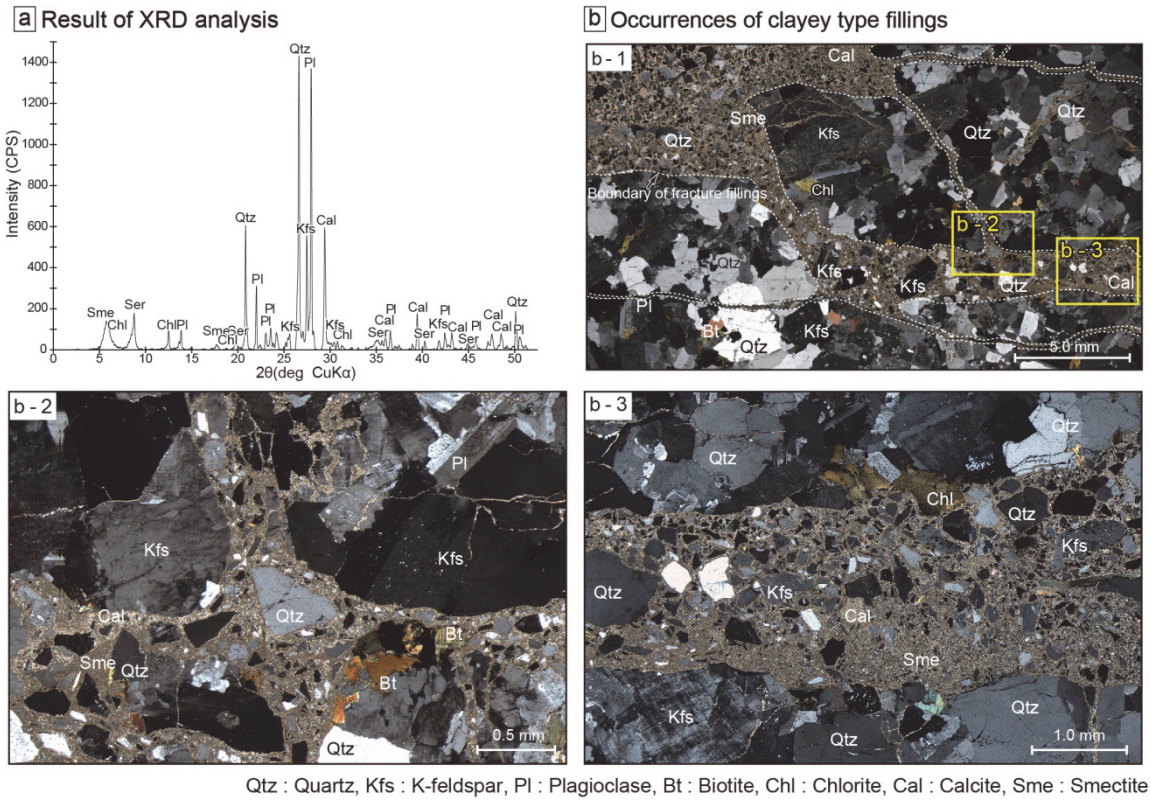

Fig. 10 (a) Results of XRD analysis of unconsolidated clayey fillings and (b) their microscopic occurrences. (b-1) Clayey-type fillings are present in microcracks. (b-2) Long axes of fragments showing similar orientations around the fracture surface. (b-3) The fragment size depends on distance from the microcrack surface; small and large fragments appear near the microcrack surface and in the core of clayey fillings, respectively. After Ishibashi et al. (2016).

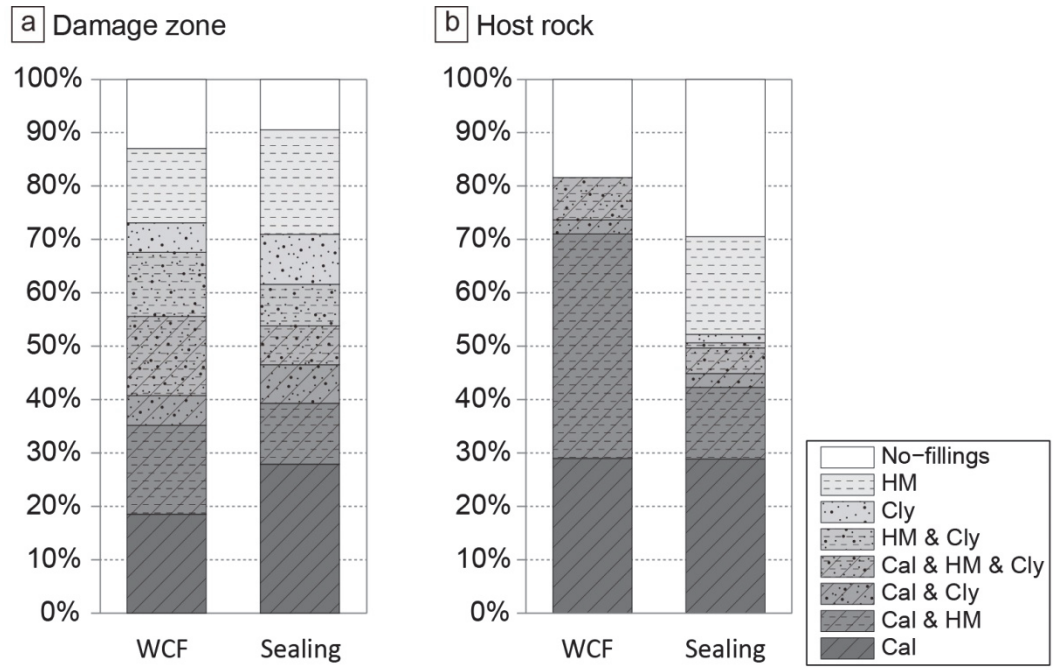

Fig. 11 (a) Relations between the WCFs and fracture fillings in the fault damage zone and in (b) host rock. Sealing refers to sealed (non-WCF) features.

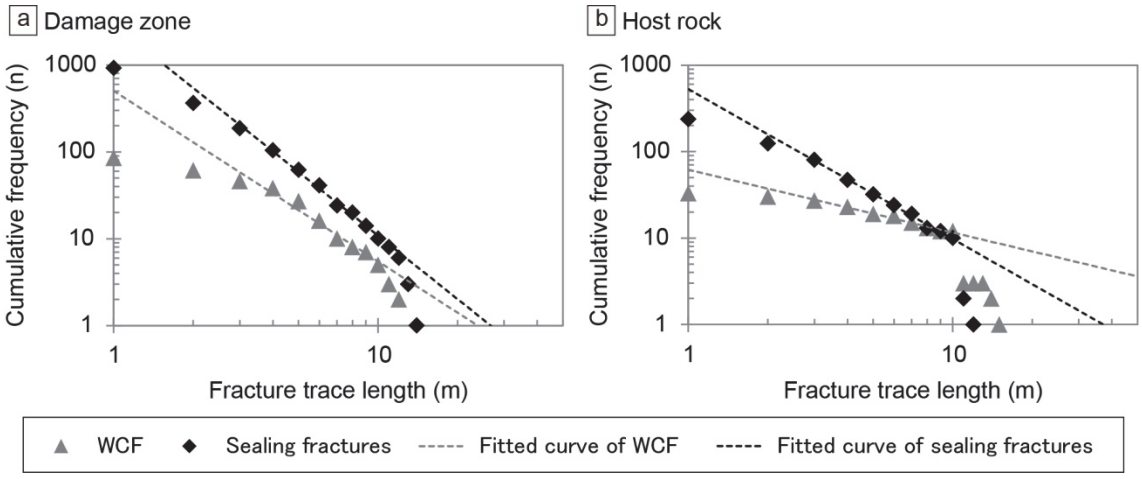

Fig. 12 (a) Length distributions of fracture traces in the damage zone and in (b) host rock. WCF fractures are larger than the sealing fractures in both areas.

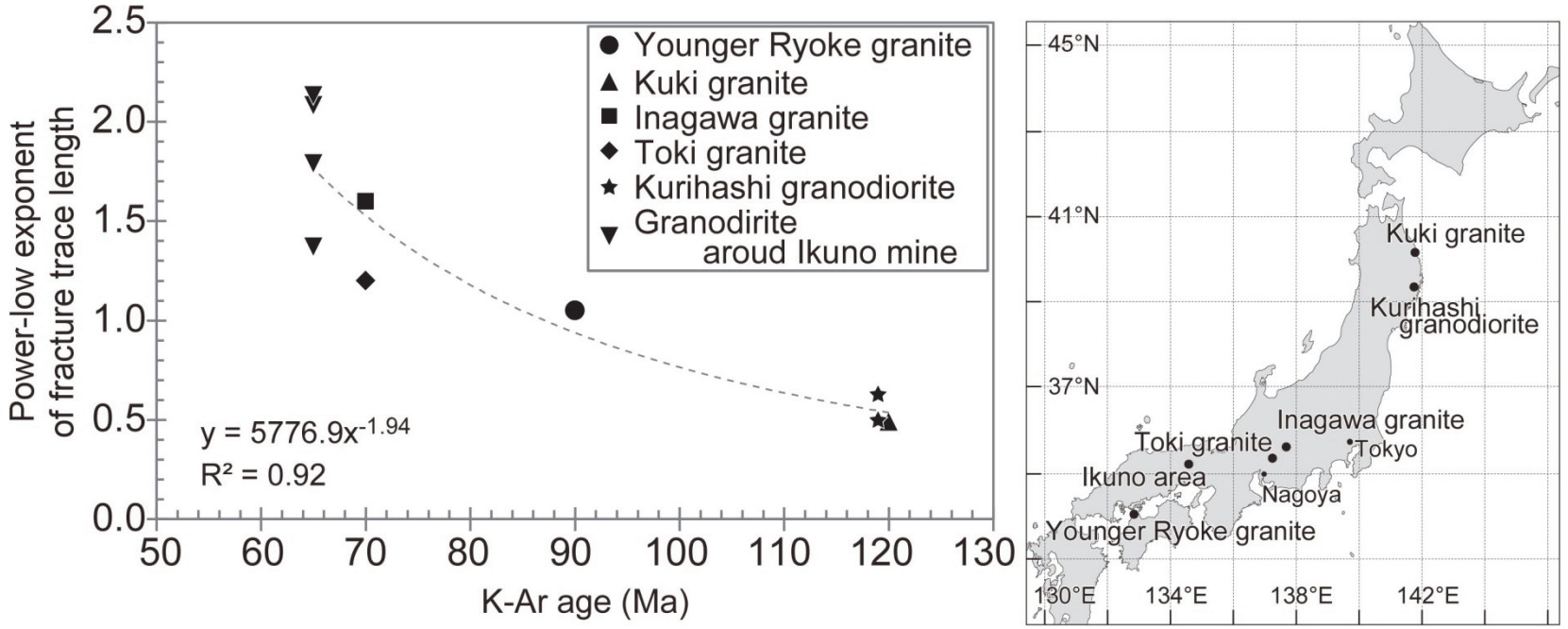

Fig. 13 Relations between power-law exponents of background fracture trace length and whole rock K–Ar ages of each granitic rock at the specified locations. The power-law exponents are the gradients of trace length vs. cumulative density of fracture plots. A high power-law exponent indicates high density of the relatively short trace length fractures. This result indicates that the trace lengths of fractures develop (expand) with older age of the granitic rocks.

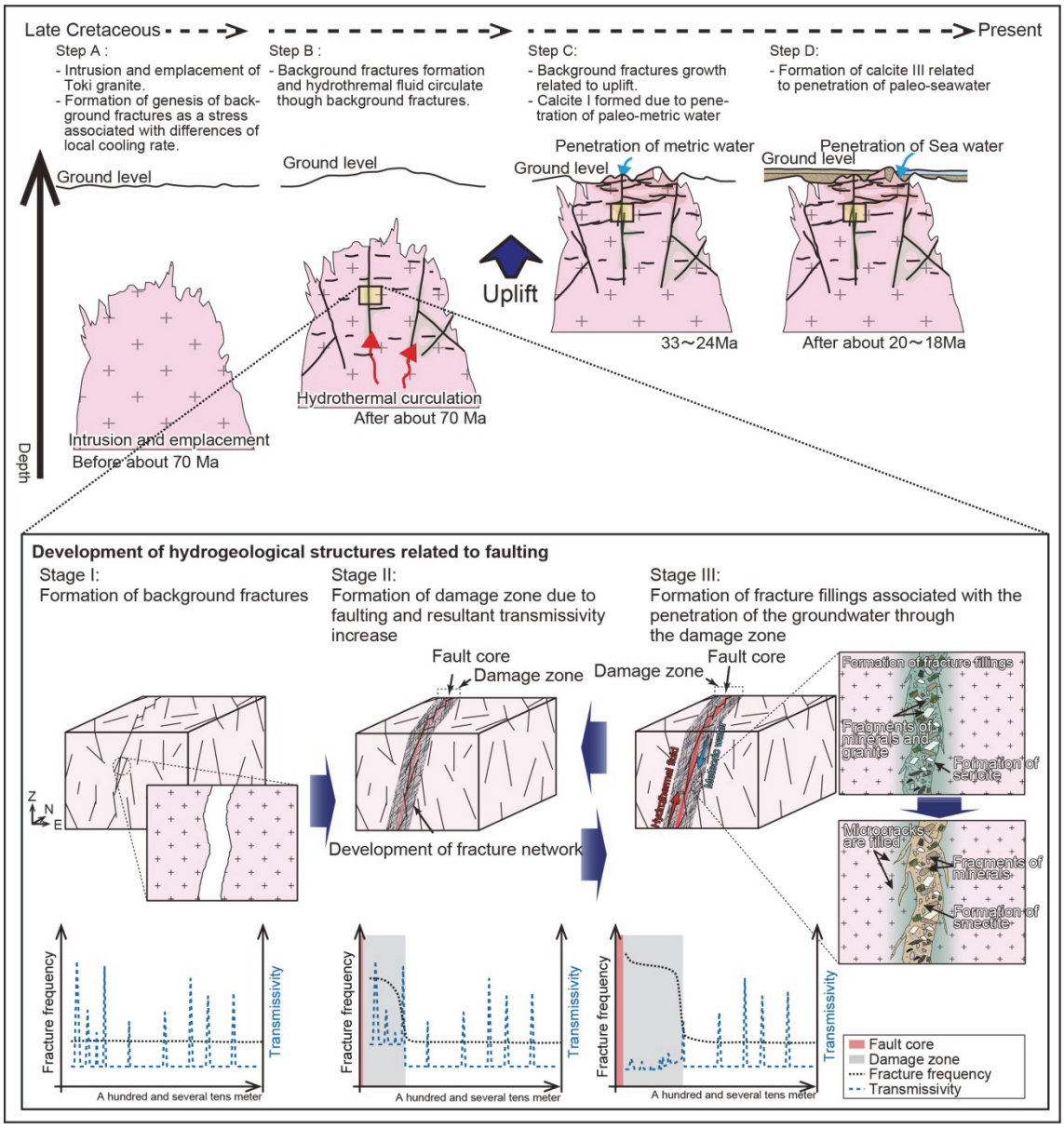

Fig. 14 Schematic of the background fracture development and long-term behavior of the fault damage zone as a hydrogeological structure. Modified from Ishibashi et al. (2014, 2016).

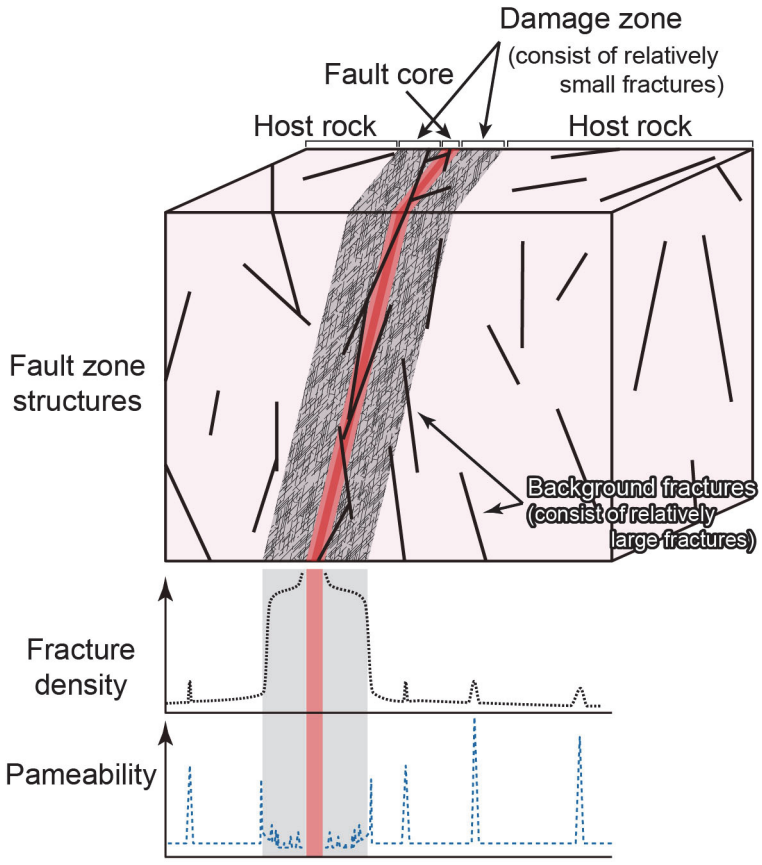

Fig.15 Schematic of the physical properties in the fault damage zone based on this study.

Table 1: Underground environment of stable continental region and orogenic field. The Forsmark in central Sweden and Olkiluoto in western Finland are representative stable continental regions, and the Mizunami Underground Research Laboratory (MIU) site in central Japan is an orogenic field.

	Forsmark central Sweden	**Olkiluoto western Finland**	**MIU (this study area) cantal Japan**
Age of Granitic rock	1910 - 1750 Ma	1873 - 1778 Ma	70 Ma
Fracture frequency at the upper part	1.02 - 3.17 m^2/m^3	1.22 - 3.15 m^2/m^3	3.37 - 7.48 m^2/m^3
Fracture frequency at the lower part	0.54 - 0.77 m^2/m^3	0.32 - 0.82 m^2/m^3	1.36 m^2/m^3
Frequency of the fault	0.62 n/km^2	3.93 n/km^2	9.75 n/km^2
Cooling rate duaring the brittle-ductile transition	0.6-4 °C/Ma	0.5-1.0 °C/Ma	7-9 °C/Ma

Table 2: Investigation methods and their objectives. Modified from Ishibashi et al. (2016).

Investigation	***Method***	***Objective***
Borehole investigation	・Core logging ・Borehole television survey ・Hydraulic packer test	・Fracture frequency (distribution) ・Fracture orientation ・Hydraulic transmissivity
Geological investigations in the gallery		
・Scan-line investigation	・Fracture characterization ・Measurement of fracture orientation	・Fracture frequency (distribution) ・Distribution of fracture fillings ・Fracture orientation
・Gallery-wall mapping	・Sketch of all fractures ・Measurement of inflow rate from WCF	・All fracture distribution ・Trace length of fractures ・Distribution of fractures with groundwater inflow and their inflow rate
Laboratory test	・Microscopy ovservation ・XRD analysis ・isotopic analysis	・Occurrence of minerals ・Mineral species ・$\delta^{18}O$ and $\delta^{13}C$

Table 3: Isotopic compositions of calcite on the fracture surface

Sample	Calcite			Solution from which calcite precipitated			
	δ13C (‰ PDB)	δ18O (‰ PDB)	δ18O (‰ SMOW)	δ13C *1 (‰ PDB)	δ18O *2 (‰ SMOW)	Temp *3 (°C)	Temp *4 (°C)
Cal I - (1)	-6.96	-17.86	12.45	-8.79	-16.47	66.51	146.82
Cal I - (2)	-9.49	-21.08	9.13	-11.32	-19.69	92.33	198.86
Cal II - (1)	-4.14	-10.10	20.45	-5.98	-8.70	21.75	69.83
Cal II - (2)	-15.79	-10.17	20.38	-17.61	-8.77	22.08	70.35
Cal II - (3)	-16.03	-7.90	22.72	-17.85	-6.49	12.01	54.78
Cal II - (4)	-9.04	-8.86	21.73	-10.87	-7.45	16.14	61.09
Cal II - (5)	-8.84	-8.81	21.78	-10.67	-7.40	15.92	60.76
Cal II - (6)	-25.08	-9.85	20.71	-26.88	-8.45	20.59	68.01
Cal II - (7)	-9.64	-5.98	24.70	-11.47	-4.57	4.28	43.16
Cal III - (1)	-4.86	-10.53	20.01	-6.70	-9.13	23.77	73.03
Cal III - (2)	-7.27	-10.04	20.51	-9.10	-8.64	21.47	69.39
Cal III - (3)	-4.28	-9.31	21.26	-6.12	-7.90	18.14	64.19
Cal III - (4)	-5.16	-7.56	23.07	-7.00	-6.15	10.60	52.62
Cal IV - (1)	-12.87	-10.73	19.80	-14.69	-9.33	24.73	74.55
Cal IV - (2)	-9.22	-13.44	17.01	-11.05	-12.04	38.70	97.35
Cal IV - (3)	-9.27	-7.57	23.06	-11.10	-6.16	10.64	52.69
Cal IV - (4)	-16.55	-11.08	19.44	-18.37	-9.68	26.43	77.25
Cal IV - (5)	-14.08	-8.90	21.69	-15.90	-7.49	16.31	61.36
Mix - (1)	-9.56	-12.84	17.62	-11.39	-11.44	35.43	91.91
Mix - (2)	-8.58	-9.83	20.73	-10.41	-8.43	20.50	67.87

*1: Calculated using α=1.00185 at 20℃ (Emrich et al., 1970)

*2: Calculated using α=1.0294 at 20 ℃ (O' Neil, 1969).

*3: Calculated using which was estimated assuming $\delta^{18}O$ of groundwater (8.3%).

*4: Calculated using which was estimated assuming $\delta^{18}O$ of seawater (0%).

Table 4: Fracture features in and around the damage zone at levels GL−300 m and GL−500 m. Modified from Ishibashi et al. (2016)

Depth	*Data*	*unit*	*Damage zone* (*-300 m: until about 100 m*, *-500 m: until about 60 m*)	*Around damage zone* (*-300 m: over about 100 m*, *-500 m: over about 60 m*)
-300 m	Average number of fractures			
	Borehole investigations	(n/m)	3.34	1.14
	Scan-line investigations	(n/m)	1.37	-
	Gallery-wall mapping	(n/m^2)	0.91	-
	Trace length < 4.0m	(%)	93.02	-
	Trace length ≥ 4.0m	(%)	6.98	-
	WCF	(%)	11.44	
	Fracture fillings			
	no-fillings	(n/m)	0.06 (4.44 %)	-
	Cal	(n/m)	0.09 (6.22 %)	-
	Ser	(n/m)	0.05 (4.00 %)	-
	Cly	(n/m)	0.01 (0.44 %)	-
	Cal & Ser	(n/m)	0.96 (69.78 %)	-
	Ser & Cly	(n/m)	0.02 (1.78 %)	-
	Cal & Cly	(n/m)	0.00 (0.00 %)	-
	Cal & Ser & Cly	(n/m)	0.18 (13.33 %)	-
	Hydraulic transmissivity of each fracture	(m^2/s)	1.02E-11 - 1.01E-4	6.54E-11 - 2.05E-9
-500 m	Average number of fractures			
	Borehole investigations	(n/m)	6.22	1.96
	Scan-line investigations	(n/m)	2.88	1.23
	Gallery-wall mapping	(n/m^2)	1.01	0.24
	Trace length < 4.0m	(%)	92.80	87.95
	Trace length ≥ 4.0m	(%)	7.20	12.05
	WCF	(%)	6.89	8.76
	Fracture fillings			
	no-fillings	(n/m)	0.11 (3.82 %)	0.14 (11.50 %)
	Cal	(n/m)	0.53 (18.58 %)	0.39 (31.86 %)
	Ser	(n/m)	0.58 (20.00 %)	0.23 (18.58 %)
	Cly	(n/m)	0.24 (8.24 %)	0.00 (0.00 %)
	Cal & Ser	(n/m)	0.50 (17.35 %)	0.27 (22.12 %)
	Ser & Cly	(n/m)	0.31 (10.88 %)	0.00 (0.00 %)
	Cal & Cly	(n/m)	0.25 (8.82 %)	0.05 (4.42 %)
	Cal & Ser & Cly	(n/m)	0.36 (12.35 %)	0.14 (11.50 %)
	Hydraulic transmissivity of each fracture	(m^2/s)	3.71E-11 - 2.78E-9	1.33E-10 - 6.18E-6

no-fillings : fractures without fillings, Cal : calcite, Ser : sericite, Cly : clayey type fillings